CHAPTER IV
SURFACE-MODIFIED CALCIUM CARBONATE PARTICLES BY ADMICELLAR POLYMERIZATION TECHNIQUE TO BE USED AS FILLER FOR ISOTACTIC POLYPROPYLENE

4.1 Abstract

The formation of thin films on solid surfaces has been a subject of intense studies in recent years because of a wide variety of possible applications. Admicellar polymerization was used to produce a thin polypropylene (PP) film on the surface of calcium carbonate ($CaCO_3$) particles using sodiumdodecylsulfate (SDS) as the surfactant template and sodium peroxodisulfate ($Na_2S_2O_8$) as the thermal initiator. In the formation of PP, the effects of process conditions (i.e. pH, equilibrium time for adsorption, salt concentration, and surfactant concentration) were studied to obtain optimum conditions for the admicellar polymerization of PP onto $CaCO_3$ particles. The admicellar-treated $CaCO_3$ was characterized by Fourier-transformed infrared spectroscopy (FT-IR), particle size analysis, and gravimetric analysis (percentage of weight loss). Non-isothermal crystallization studies indicate that surface treatment of $CaCO_3$ particles reduced the nucleating ability of the $CaCO_3$ particles. WAXD results suggested that surface-treated $CaCO_3$ resulted in the reduction of degree of crystallinity of iPP matrix. The effect of $CaCO_3$ of various surface characteristics on mechanical properties of $CaCO_3$-filled isotactic polypropylene (iPP) composites was investigated. Both stearic acid-coated and admicellar-treated $CaCO_3$ reduced tensile strength at yield, Young's modulus, and flexural strength, while improved strain at yield and impact strength, of the composites. Observation of the fracture surfaces of the composites by scanning electron microscopy (SEM) iPP revealed an improvement in $CaCO_3$ dispersion as a result of the surface treatment.

KEYWORDS: Admicellar polymerization/ Composite/ Calcium carbonate/ Isotactic polypropylene/

4.2 Introduction

Polymers in their combination with various additives and fillers are popular materials for making household articles or used directly as construction and engineering materials. Usually, polymers are filled with crystalline minerals, a class of materials called polymeric composites [1]. Composites are heterogeneous substances consisting of two or more materials which do not lose the characteristics of each component. This combination of materials brings about new desirable properties. Industrially, mineral filler additives are added into the polymer matrix not only to reduce the cost, but also to improve other properties, such as mechanical properties, dimensional stability, and surface hardness. The effect of fillers on mechanical and other properties of the composites depends strongly on their shape, size and size distribution of the primary particles and their aggregates, surface characteristics, and degree of dispersion [2].

Of the various mineral fillers used, calcium carbonate ($CaCO_3$) is the most common one, due mainly to its availability in readily usable form and low cost [3]. However, the incompatibility of its high energetic hydrophilic surface with the low-energy surface of hydrophobic polymers, such as polyethylene (PE) and polypropylene (PP), is a problem to be solved before it can be used as a functional filler. For this and other reasons, the surface of calcite is often rendered organophilic by a variety of surface modifiers such as silane, titanate, phosphate, and stearic acid. Commonly, stearic acid is the most common surface modifier, while use of other types seem to be limited by their relatively high cost. One question regarding the efficiency of stearic acid as the surface modifier for improving adhesion and dispersion between $CaCO_3$ and the polymer matrix is the level of its compatibility with the matrix molecules.

On the basis of "like dissolves like," the interfacial interaction (adhesion) between materials of a similar chemical nature is considered superior to that of any other type. Let us imagine if there is a technology that can put a thin layer of the matrix material to act as the surface modifier for $CaCO_3$, what would be like for the surface-modified $CaCO_3$ to perform in the matrix? In fact, one such technique,

admicellar polymerization [4], has been developed. Admiceilar polymerization technique is based on physically adsorbing surfactants onto a substrate. Nevertheless, at right conditions, the admicellar layer adheres well to the substrate via ionic interactions. The structure and properties of such an ultrathin organic film have a strong influence on the final properties of the composites because this film represents the interface between the two phases that are heterogeneous in nature. It also determines the particle-particle as well as the particle-matrix interactions and controls the buildup of the interphase.

In the present study, the admicellar polymerization technique is used to produce ultrathin polypropylene film on the surface of $CaCO_3$ particles. The film-forming process includes four major steps (see Figure 4.1): (i) the adsorption of a thin admicellar layer of surfactants, e.g. sodium dodecylsulfate (SDS), on $CaCO_3$ substrate; (ii) the adsolubilization of propylene gas monomer into the admicelles; (iii) The initiation of polymerization within the admicellar bilayers; (iv) the washing of the treated $CaCO_3$ to remove as much of the outer surfactant layer as possible in order to expose the film.

The main purpose of this study is to investigate the effect of $CaCO_3$ particles which were coated with a thin layer of polypropylene on mechanical properties and non-isothermal crystallization characteristic of resulting isotactic polypropylene (iPP) composites in comparison with the untreated and stearic acid-coated $CaCO_3$ particles.

4.3 Experimental

4.3.1 Materials

A commercial grade of isotactic polypropylene (iPP) (HP500N) was courteously supplied by HMC Polymers Co., Ltd. (Thailand). HP500N was a homopolymer grade with density and melt-flow rate (MFR) values being about 0.90 $g \cdot cm^{-3}$ and 12 $dg \cdot min^{-1}$, respectively. Calcium carbonate ($CaCO_3$) (CALOFIL1000; average particle size = 1.2 μm) and stearic acid-coated $CaCO_3$ (HICOAT1010; average particle size = 1.2 μm), used as the fillers for iPP, were courteously supplied by Calcium Products Co., Ltd. (Thailand).

Polymerization grade propylene gas (purity = 99.5%), used as the monomer, was purchased from Linde Gas Singapore Ltd.. Sodium dodecyl sulfate (purity = 94-98%), use as an anionic surfactant template, was purchased from Carlo Erba Reagenti (Italy). Sodium persulfate (purity = 99.0%+), used as the water-soluble initiator, was purchased from Fluka (USA). Xylene (AR grade), used as the extracting solvent, was purchased from Labscan (Asia) (Thailand). Sodium chloride (purity = 99.9%+) was purchased from Carlo Erba Reagenti (Italy). Sodium hydroxide (AR grade) and hydrochloric acid (37 wt.% aqueous solution; AR grade), used as pH adjuster, were purchased from Labscan (Asia) (Thailand). All of the chemicals were used as-received.

4.3.2 Methodology

4.3.2.1 Determination of Point of Zero Charge (PZC) of $CaCO_3$

The change in the surface charge of $CaCO_3$ particles with pH is important to determine the surfactant adsorption. Electrophoretic mobility was used to determine the surface charge of the $CaCO_3$ particles at various pH values. The colloidal $CaCO_3$ was diluted in 100 ml distilled water. The pH of the solution was adjusted either by 0.1 M NaOH or HCl and was left to equilibrate for 1 day. The electrophoretic mobility of the $CaCO_3$ particles was observed at room temperature with a Zeta potential meter 3.0.

4.3.2.2 Determination of Amount of SDS Adsorbed on $CaCO_3$

A solution of SDS of a desired concentration, pH (i.e. less than the pH at PZC), and salt concentration (i.e. 0.00-0.50 M) was first prepared. A 10 ml aliquot of the solution was pipetted into a 24-ml vial containing 1 g of neat $CaCO_3$ particles. The pH of the solution was adjusted with either HCl or NaOH aqueous solutions. The sealed vial was shaken at 150 rpm at room temperature for a set time that determined the equilibrium adsorption. The amount of SDS adsorped on $CaCO_3$ was calculated from the difference between the initial and final concentration of the SDS solution. The concentration of the SDS solution was determined by a KRÜSS DSA10 Mk2 drop shape analysis system. Based on the interfacial tension obtained, the SDS concentration was finally determined from a

predetermined calibration curve between the interfacial tension and the SDS standard concentration.

4.3.2.3 Determination of Adsorption Isotherm of SDS on CaCO₃

The adsorption isotherms of SDS on $CaCO_3$ particles were obtained by exposing 1 g of $CaCO_3$ to 10 ml of SDS solution of a specified initial concentration. The mixture was equilibrated at room temperature for a set time in a sealed 24-ml vial. The pH of the solution was pre-adjusted and NaCl was pre-dissolved as stated earlier. The amount of SDS in the supernatant liquid was measured by the drop shape analysis system using the same procedure as described above. The initial SDS concentration in this experiment was varied from 40 to 20,000 µM, which covered the regions below and above the CMC of SDS.

4.3.2.4 Admicellar Polymerization of Propylene onto CaCO₃

Pressure drop of propylene gas during adsolubilization and polymerization: before determining the pressure drop for adsolubilization and polymerization, the amount of propylene dissolved in water was first determined by means of a "blank" in order to find out the exact amount of propylene solubilized into the surfactant bilayers. A 1,200 ml of water containing pre-determined amount of NaCl at a specified pH as in the above experiments was poured into a Parr reactor which was then closed and sealed. After drawing a vacuum from the reactor, propylene gas was introduced and adjusted to a desired pressure at a temperature between 30 and 70°C (corresponding to the adsolubilization and admicellar polymerization conditions). The transient decrease of the pressure was recorded for further analysis

• *Admicellar polymerization process*: polymerization of propylene onto $CaCO_3$ was carried out using sodium persulfate as the initiator. A 120 g of $CaCO_3$ particles was put into the Parr reactor. A 1,200 ml aqueous solution of SDS of a desired initial concentration was fed into the reactor and the mixture was adjusted for its pH and NaCl content as previously stated. The desired initiator to surfactant ratio was 3:1. The reactor was sealed and vacuumed. After this, propylene gas was introduced into the reactor and the pressure was adjusted to 140 psi. For the adsolubilization process, the mixture was stirred at 150 rpm for a set time at 30°C. If a pressure drop was observed, the reactor was then repressurized to

140 psi before the admicellar polymerization could begin. During polymerization, the temperature of the mixture was 70°C and the stirrer speed was adjusted to 150 rpm. The transient decrease of the pressure was recorded and the polymerization was considered complete when the pressure within the reactor was constant, after which time the temperature of the reactor was cooled down to room temperature. The supernatant liquid was carefully decanted from the reactor and the treated $CaCO_3$ particles were washed several times with distilled water and later dried in a vacuum oven at 80°C overnight.

4.3.3 Characterization and Testing

4.3.3.1 Characterization of The Coated Film

FT-IR was used to characterize the as-polymerized polypropylene film. The coated film on treated $CaCO_3$ was extracted by boiling xylene. After evaporation of xylene, the remaining polymer was coated on a silinide disk for further analysis in a Thermo Nicolet Nexus 670 FT-IR spectrometer.

4.3.3.2 Particle Size Analysis of $CaCO_3$ Particles

A Malvern MastersizerX particle size analyzer was used to determine the size of the as-received, untreated, and admicellar-treated $CaCO_3$ particles.

4.3.3.3 Gravimetric Analysis (Percentage of Weight Loss)

The difference in the weight of $CaCO_3$ particles of different surface characteristics before and after burning in a furnace at 600°C for 1 h was used to determine the organic content that was present on the $CaCO_3$ particles, according to the following relationship:

$$\% \text{ weight loss} = \frac{\text{weight of } CaCO_3 \text{ (before burning} - \text{after burning)}}{\text{weight of } CaCO_3 \text{ after burning}} \times 100$$

$CaCO_3$ particles were dried in oven at 60°C for 24 h and weighted before calcination.

4.3.3.4 Polymer Composite Preparation

Compounds of iPP and 30 wt.% of $CaCO_3$ particles of different surface characteristics were carried out first by pre-mixing for 10 min in a

tumble mixer and melt-mixed in a Collin ZK25 self-wiping, co-rotating twin-screw extruder operating at a screw speed of 50 rpm and a temperature profile of 190 (die), 190 (zone 4), 180 (zone 3), 170 (zone 2), 160 (zone 1), and 80°C (feed zone). The composite extrudates were water-cooled and later pelletized by a Planetrol 075D2 pelletizer. The composite pellets were dried at 60°C overnight and later injection-molded into specimens for mechanical tests using an ARBURG Allrounder® 270M injection molding machine. The temperature settings (from the feed zone to the nozzle) were 160, 170, 175, 185, and 190°C, respectively. The injection pressure was 1,000 bars and the dwelling pressure was 700 bars. Prior to the mechanical tests, all of the test specimens were conditioned under ambient conditions for 7 days.

4.3.3.5 Differential Scanning Calorimetry Measurements

Non-isothermal crystallization and melting behavior of $CaCO_3$-filled iPP samples was investigated on a Perkin-Elmer Series 7 differential scanning calorimeter (DSC). Temperature calibration was performed using an indium standard (T_m^o = 156.6°C and ΔH_f^o = 28.5 J/g). Each sample of 3 to 6 mg in weight, cut from the prepared compressed films, was sealed in an aluminum sample holder. The experimental procedure started with melting each sample at 200°C for 5 min and then cooling it to 30°C at a rate of 10°C/min. After that, the sample was immediately subjected to heating at a rate of 20°C/min to 190°C. Both the crystallization exotherm and the melting endotherm were recorded for further analysis. All measurements were carried out in a nitrogen atmosphere.

4.3.3.6 Crystal Structure and Crystallinity Measurements

A wide-angle X-ray diffraction (WAXD) technique was used to determine the crystal modification and the apparent degree of crystallinity for both neat and $CaCO_3$-filled iPP samples prepared according to the conditions set forth for DSC measurements but without a subsequent heating step. Each sample was removed from the DSC sample holder and pasted onto a glass sample holder. The WAXD intensity patterns of the sample were then collected on a Rigaku Rint2000 diffractometer (CuK$_\alpha$ radiation, λ = 1.54 Å), equipped with computerized data collection and analytical tools. The X-ray source was operated at a voltage of 40 kV and a filament current of 30 mA.

4.3.3.7 Mechanical Properties Measurements

Tensile testing: the tensile strength of the $CaCO_3$-filled iPP composites were determined using an Instron universal testing machine. The testings were carried out according to ASTM D638-91 using a 100 kN load cell and 50 mm/min crosshead speed. The results from these tests were reported as averages of the data taken from at least 10 specimens..

Flexural testing: the flexural strength of the composites were measured using an Instron universal testing machine according to ASTM D790-92 in the three-point bending mode. Measurements were carried out using a 5 kN load cell, 11.52 mm/min crosshead speed, and a 43.2 mm support span. The results from these tests were reported as averages of the data taken from at least 15 specimens.

Impact testing: Izod impact strength was measured using a Zwick pendulum impact tester instrument with 2.7 joules pendulum according to ASTM D256-90b. The results from these tests were reported as averages of the data taken from at least 15 specimens.

4.3.3.8 Morphology Observation of Fracture Surface

A JEOL JSM-5200 scanning electron microscope (SEM) was used to observe the microstructure of the impact-fractured surface of selected specimens obtained after the impact testing. Each selected specimen was cut about 2 mm below the fractured surface and the cut piece was stuck onto a brass stub. Prior to observation under SEM, each sample was gold-coated using a JEOL JFC-1100E ion sputtering device to enhance the conductivity of the surface. The average percentage area of $CaCO_3$ particles observed on the SEM images was analyzed by Semafore 4.0 software and was used to assess the dispersion of $CaCO_3$ particles within the iPP matrix.

4.4 Results and Discussion

4.4.1 Determination of Optimum Conditions for SDS Adsorption on $CaCO_3$

4.4.1.1 The Point of Zero Charge (PZC) of $CaCO_3$

The PZC is determined from the intersection of the electrophoretic mobility curve and the zero axis. As shown in Figure 4.2, the PZC

on the surface of $CaCO_3$ particles was observed at the pH of 11.4 at room temperature.

Martínez-Luévanos *et al.* (1999) reported that the natural tendency of the $CaCO_3$-water system attained equilibrium at pH 8.3 [5].

$$CaCO_3(s) + 2H^+ = Ca^{2+} + CO_2(g) + H_2O$$

In this study, the anionic surfactant, SDS, was employed, so the pH was adjusted to 8 to ascertain a positive charge on the $CaCO_3$ surface onto which SDS molecules would be adsorbed by orienting their negatively-charged head groups towards the positively-charged surface of $CaCO_3$ surface (i.e. due to the electrostatic attraction).

4.4.1.2 The Equilibrium Time for SDS Adsorption on $CaCO_3$

The SDS adsorbs readily on $CaCO_3$ at room temperature and pH 8 (Figure 4.3). The initial SDS concentration used was 20 mM which is well above its CMC. The adsorption of SDS was found to decrease very rapidly to reach a minimum at about 12 h, after which it increased and became constant at about 40 μmol/g of $CaCO_3$ after about 18 h. Therefore, in subsequent experiments, the adsorption step was carried out for 24 h to ensure equilibrium adsorption.

4.4.1.3 The Effect of Electrolyte on the Adsorption of SDS on $CaCO_3$

The equilibrium adsorption of SDS varied with the amount of electrolyte added at a fixed pH of 8 (Figure 4.4). In this experiment, the initial concentration of SDS was 20 mM. The results show that the adsorption of SDS on $CaCO_3$ increased sharply with increasing NaCl concentration in the range 0.2-0.3 M, but it increased moderated at higher NaCl concentration. The Na^+ counterions help reduce the negative charges on $CaCO_3$ surface and reduce the repulsion of surfactant headgroups, resulting in greater SDS adsorption when NaCl is added. Similar results were obtained by Pongprayoon *et al.* (2002) [6]. In this work the amount of SDS adsorption on $CaCO_3$ was found to increase from around 40 μmol/g of $CaCO_3$ with no salt addition to around 68 μmol/g of $CaCO_3$ with 0.3 M NaCl.

4.4.2 Determination of the Adsorption Isotherm of SDS on $CaCO_3$

The adsorption isotherm of SDS on $CaCO_3$ at pH 8 and a fixed salt concentration of 0.3 M are presented in Figure 4.5. It can be seen that the adsorption

isotherm of SDS on $CaCO_3$ conforms to curve shapes typical of the adsorption of an ionic species on a solid substrate. The amount of SDS adsorbed on $CaCO_3$ was found to initially increase sharply with increasing SDS concentration. As the SDS concentration increased further, the slope started to decline, leading eventually to a constant valve. The point at which the curves converged to a plateau value corresponded to the CMC of the system.

4.4.3 Admicellar Polymerization of Propylene Gas Monomer on $CaCO_3$

For the admicellar polymerization of propylene onto $CaCO_3$, the amount of SDS used was determined from the adsorption isotherm which was 30 μmol/g of $CaCO_3$ for the SDS adsorption on $CaCO_3$ and 500 μM for the equilibrium SDS concentration in the supernatant liquid and the other system was 15 μmol/g of $CaCO_3$ for the SDS adsorption on $CaCO_3$ and 200 μM for the equilibrium SDS concentration in the supernatant liquid. These values were lower than the experimentally observed CMC of the system to avoid emulsion polymerization to occur.

Table 4.1 compares the pressure drop of propylene at two different admicellar polymerization conditions. It can be seen that higher surfactant concentration resulted in higher propylene pressure drop. The difference in propylene pressure drop is a measure of polymerization occurring within the admicelles. It can be concluded that more admicellar polymerization occurred in the system with higher surfactant concentration.

4.4.4 Characterization of Coated Film

To confirm that polypropylene has been successfully coated on $CaCO_3$ particles by admicellar polymerization, the solid residue from xylene extraction was characterized by FT-IR, from which the data obtained was compared with that obtained from pure SDS and pure atactic polypropylene (aPP). The FT-IR spectra of aPP, solid residue, and SDS are shown in Figure 4.6a and Table 4.2 summarized characteristic peaks observed for solid residue.

According to Figure 4.6a, it is obvious that FT-IR spectrum of the solid residue not only shows a bunch of peaks corresponding to aPP structure, but

also strong peaks at 1,050-1,120 and 1,220-1,300 cm^{-1} were found, assignable to the stretching vibrational bands of sulfate groups (as show in Figure 4.6b, the FT-IR spectrum of initiator, $Na_2S_2O_8$), which possibly came from initiator and existed at the chain ends. The strength of sulfate peaks suggests that the synthesized polymer chains have relatively low molecular weight as the ratio of chain ends to repeating unit is high.

4.4.5 Particle Size Analysis of CaCO₃ Particles

Particle size results of the various types of surface-treated $CaCO_3$ are shown in Figure 4.7. When compared to the results obtained for untreated $CaCO_3$, admicellar-treated $CaCO_3$ resulted in the lower deviation of particle size, indicating that the surface modification by admicellar polymerization helped decrease the degree of agglomeration of the $CaCO_3$ particles.

4.4.6 Gravimetric Analysis (Percentage of Weight Loss)

Table 4.3 summarizes the percentage of weight loss of the various types of surface-treated $CaCO_3$ particles.

It can be seen that untreated $CaCO_3$ particles had the lowest weight loss as expected. The highest percentage of weight loss was stearic acid-coated $CaCO_3$ particles which was commercially available $CaCO_3$ grade.

The percentage of weight loss of the various types of surface-treated $CaCO_3$ is shown graphically in Figure 4.8. This graph clearly shows that the admicellar-treated (PP-coated) $CaCO_3$ had slightly greater weight loss in comparison with the untreated $CaCO_3$ particles. Furthermore, the percentage of weight loss increased with increasing surfactant concentration, indicating more aPP was coated on the surface of $CaCO_3$. This result corresponded well with the propylene pressure drop results.

4.4.7 Non-isothermal Crystallization and Melting Behavior

Figure 4.9a and 4.9b shows non-isothermal crystallization exotherms for neat and $CaCO_3$-filled iPP samples with various types of surface treatment (as-received, stearic acid-coated, untreated, and admicellar-treated) at 2 and 30 wt.% of

CaCO$_3$ contents (recorded at a cooling rate of 10°C/min), respectively. Apparently, the crystallization (peak) temperature (T_{cl}) for the neat iPP sample was observed at about 112.8°C. The incorporation of CaCO$_3$ particles shifted the T_{cl} value toward a higher temperature. Figure 4.9b shows two types of crystallization exotherm. The first is the single-peak type (the peak temperature of the low-temperature peak denotes T_{cl}) and the second is the double-peak type (the peak temperature of the high-temperature peak denotes T_{ch}), which was only found for iPP sample filled with 30 wt.% untreated CaCO$_3$ particles.

The occurrence of double crystallization behavior for 30 wt.% untreated CaCO$_3$-filled iPP samples may by a result of the self-nucleation effect, likely attribute to the residual iPP crystallites entrapped along the rough surface of untreated CaCO$_3$ particles. Due to this entrapment, some of these crystallites may survive through the melting process, and during subsequent cooling, they can act as predetermined nuclei to initiate crystallization. On the other hand, the crystallization exotherms recorded for iPP samples filled with 30 wt.% stearic acid-coated and admicellar-treated CaCO$_3$ particles exhibited only single crystallization exotherm. These are probably due to the decrease of iPP crystallites entrapped on the rough surface when the CaCO$_3$ surface is coated or treated with a non-nucleating substance (hence reducing the probability for these entrapped crystallites to self-nucleate the iPP melt during subsequent cooling).

Apart from the self-nucleation effect of entrapped crystallites, which is thought to be the most likely explanation for double crystallization behavior, other possible explanations may be (i) the difference of crystallization behavior on the different parts of the particle surface, and (ii) the presence of both accelerating and non-accelerating crystallized parts on the particle surface.

It should be noted that the occurrence of double crystallization behavior was also reported for iPP samples filled with 25 vol.% 1.3 μm uncoated CaCO$_3$ by Pukánszky and Fekete (1998) [7] and for sPP samples filled with high contents of 1.9 μm uncoated CaCO$_3$ particles (approx. 20-40 wt.%) by Supaphol and Harnsiri (2003) [8].

Table 4.4 summarizes the non-isothermal crystallization results observed. According to Table 4.4, the $T_{c,onset}$ values obtained for stearic acid-coated

and admicellar-treated $CaCO_3$-filled iPP samples were lower than the value for untreated $CaCO_3$-filled iPP samples at the same filler loading. Clearly, the nucleating efficiency of $CaCO_3$ was reduced by such surface treatments.

The subsequent melting endotherms for neat and $CaCO_3$-filled iPP sample with various types of surface treatment at 2 and 30 wt.% of $CaCO_3$ contents (recorded at a heating rate of 20°C/min) are shown in Figure 4.10a and 4.10b, respectively. Some samples with double melting endotherms (the low-temperature peak denotes T_{ml} and the high-temperature peak denotes T_{mh}) in their heating scans were found for 2 wt.% as-received, untreated, and admicellar-treated $CaCO_3$-filled iPP samples, in which these low-temperature melting endotherms correspond to the melting of β-phase of iPP [9].

According to Figure 4.10b, when considering the resulting T_{mh} values for iPP samples filled with various types of surface treated $CaCO_3$ particles at 30 wt.% of $CaCO_3$ contents, it is evident that the results obtained agreed particularly well with the crystallization results (see Figure 4.9b) in that the T_{mh} value obtained for untreated $CaCO_3$-filled iPP samples was higher the values for stearic acid-coated and admicellar-treated $CaCO_3$-filled iPP samples. Table 4.5 summarizes the results regarding subsequent melting behavior obtained for all of the samples studied.

4.4.8 Crystal Structure and Crystallinity

In order to observe the crystal structure and the resulting apparent degree of crystallinity of neat iPP and $CaCO_3$-filled iPP composites investigated, a WAXD technique was utilized. Figure 4.11a and 4.11b show the WAXD patterns for neat iPP and $CaCO_3$-filled iPP samples with various types of surface treatment (as-received, stearic acid-coated, untreated, and admicellar-treated) at 2 and 30 wt.% of $CaCO_3$ contents, respectively. Each sample was prepared in the DSC cell at a cooling rate of 10°C/min. For the neat iPP sample, the characteristic X-ray peaks were observed at the scattering angles 2θ of about 13.9, 16.7, 18.4, 20.9, and 21.7°. These results showed strong agreement with Zhang *et al.* (2004), in which they suggested these characteristic peaks corresponded to reflection planes at (110), (040),

(130), (111), and (041), respectively, according to monoclinic unit cell (α-form of iPP) [10].

In Figure 4.11a, the WAXD patterns of as-received, untreated, and admicellar-treated $CaCO_3$-filled iPP samples not only show the five characteristic X-ray peaks of α-form of iPP, but also observe a peak at $2\theta = 15.8°$ corresponding to the (300) crystal plane of β-form of iPP (hexagonal unit cell), indicating that as-received, untreated, and admicellar-treated $CaCO_3$ particles can act as β-nucleating agents. Moreover, the major characteristic peak of $CaCO_3$ at angle 2θ of about 29.2° (corresponded to (104) reflection plan) is evident for all $CaCO_3$-filled iPP samples.

To quantify the relative amount of β-phase versus α-phase of iPP, an empirical model was advised by Turner-Jones et al. (1964) [11], according to the following equation:

$$K_\beta = \frac{I_{(300)_\beta}}{I_{(300)_\beta} + [I_{(110)_\alpha} + I_{(040)_\alpha} + I_{(130)_\alpha}]}$$

Where $I_{(hkl)}$'s are the intensities of the peaks specific to the indicated reflections of the β-form and α-form of iPP. According to the K_β results shown in Table 4.6, the K_β value was found to decrease when the surface of $CaCO_3$ particles was coated with aPP and more aPP coated on the surface of $CaCO_3$ resulted in the greater K_β value.

Figure 4.11b shows the WAXD diffractograms of neat iPP and 30 wt.% $CaCO_3$-filled iPP samples with various types of surface-treated $CaCO_3$ particles. It is clear that, with increasing $CaCO_3$ content, the intensities of the characteristic X-ray peaks of iPP crystallites become less pronounced. Similarly, major characteristic peak of $CaCO_3$ at angle 2θ of about 29.2° was apparent and became more pronounced and intensified with increasing $CaCO_3$ content. In addition, the WAXD pattern of both 2 and 30 wt.% stearic acid-coated $CaCO_3$-filled iPP samples observe an additional characteristic X-ray peak at an angle 2θ of about 30.8°, which is attributed to dolomite and becomes more pronounced and intensified with increasing $CaCO_3$ content. This clearly indicated that the stearic acid-coated $CaCO_3$ not only contains $CaCO_3$ but dolomite as well.

The results shown in Figure 4.11a and 4.11b suggest that the presence of $CaCO_3$ particles does not alter the crystal structure of the crystallizing iPP in the

matrix. It does, however, affect the apparent degree of crystallinity, χ^{WAXD}, of the iPP matrix. By referring to the relative ratio of the integrated intensities under the crystalline peaks A_c to the integrated total intensity A_t ($A_t = A_c + A_a$, where A_a is the integrated intensity under the amorphous halo), the following equation can be derived:

$$\chi^{WAXD} = \frac{A_c}{A_c + A_a} \in [0,1]$$

It is qualitatively obvious that the WAXD degree of crystallinity, χ^{WAXD}, decreases with increasing $CaCO_3$ contents. Similarly, surface-treated $CaCO_3$ resulted in the reduction of χ^{WAXD} of iPP matrix. The observed χ^{WAXD} values for all of the samples studied are summarized in Table 4.7.

4.4.9 Mechanical Properties of CaCO₃-filled iPP Composites

The $CaCO_3$ contents of most commercial $CaCO_3$-filled polypropylene range from 20 to 40 wt.%. In this study, 30 wt.% of $CaCO_3$ was chosen for all composite materials due to the limited availability of the surface-modified $CaCO_3$ particles.

4.4.9.1 Tensile Strength

The tensile strength at yield, strain at yield, and Young's modulus results for composites made from iPP filled with $CaCO_3$ particles of various surface characteristics are shown in Tables 4.8, 4.9, and 4.10, respectively.

When compared with the results obtained for iPP filled with untreated $CaCO_3$ particles, both stearic acid-coated and admicellar-treated (PP-coated) $CaCO_3$ particles resulted in the reduction of the tensile strength of the resulting composites (Figure 4.12). The decrease in the tensile strength is probably due to the poor interfacial adhesion between the $CaCO_3$ surface and the iPP matrix, resulting in poor stress transfer across the interface. Furthermore, another possible reason for the observed decrease in the tensile strength of iPP composites filled with coated $CaCO_3$ could be the decrease in the crystallinity coupled with a lubricating/plasticizing effect of the coating material. Rybnikar (1991) showed that the ability of $CaCO_3$ particles to nucleate iPP was decreased when their surface was

modified with some surface modifier [12]. Based on the report of Rybnikar (1991), stearic acid and atactic polypropylene that were coated on the surface of $CaCO_3$ that was used in this work could also suppress the ability for the filler to nucleate iPP in the matrix.

According to Figure 4.12, the decrease in the tensile strength at yield of iPP composites filled with admicellar-treated $CaCO_3$ particles in comparison with that of iPP composites filled with the untreated $CaCO_3$ particles resulted in the increase in the observed increase in the strain at yield of these composites (see Figure 4.13). The greater the amount of the coating layers of aPP, the greater the reduction in the tensile strength at yield and, conversely, the increase in the strain at yield. Based on these results, it is reasonable to indicate that the thin coating layer of aPP on the surface of $CaCO_3$ particles help lubricate or plasticate the matrix. Similar results were observed and reported by González et al. (2002) [13] when the surface of $CaCO_3$ particles was coated with either titanate or zirconate coupling agents.

In addition, the Young's modulus of iPP composites filled with both stearic acid-coated and admicellar-treated (PP-coated) $CaCO_3$ particles was found to be lower than that of the composite filled with untreated ones (Figure 4.14). Obviously, the presence of the thin layer of either stearic acid or aPP on the surface of $CaCO_3$ particles reduced the interparticular interactions, which caused the stiffening effect due to the presence of solid particles to be suppressed.

4.4.9.2 Flexural Strength

The flexural strength of iPP composites filled with $CaCO_3$ particles of various surface characteristics is listed in Table 4.11. Obviously, the composite filled with untreated $CaCO_3$ particles showed the highest value. The results obtained correlated well with the tensile properties (see Figures 4.15).

4.4.9.3 Impact Strength

The ability for a structural part to maintain its integrity and to absorb a sudden impact is often a relevant issue when selecting a suitable material. Impact strength may be defined as toughness or the ability of a material to withstand a sharp blow. Notched Izod impact strength of iPP composites filled with $CaCO_3$

particles of various surface characteristics was investigated and the results are summarized in Table 4.12.

According to Figure 4.16, the impact strength of iPP composites filled with admicellar-treated $CaCO_3$ particles was better than that of iPP composites filled with untreated ones and increasing the amount of the coating aPP layer resulted in an improvement in property value. However, when comparing with the property values of iPP composites filled with as-received and stearic acid-coated $CaCO_3$ particles, those of iPP composites filled with untreated and admicellar-treated $CaCO_3$ particles were lower. This could be a result of the lower amount of the coating layer.

The observed increase in the impact resistance of admicellar-treated $CaCO_3$-filled iPP composites incomparison with that of untreated $CaCO_3$-filled iPP composites could attribute to the lubricating or plasticizing action of the coating layer. Not only such a surface treatment reduces the surface energy, it also help reduces interparticular interactions of $CaCO_3$ particles, which all led to better dispersion with a low degree of agglomeration of $CaCO_3$ particles [Maiti and Mahapatro (1991)] [14]. As a result, the impact energy is more uniformly distributed and the effect is the observed better impact resistance (Silva et al., 2002) [15]. Interestingly, the composites made from stearic acid-coated $CaCO_3$ had the highest impact strength among all of the samples investigated. Riley et al. (1990) reported that, for $CaCO_3$-filled iPP composites, the surface coating on $CaCO_3$ particles aids the dispersion of filler in the polymer matrix, rendering a large number of discrete particles that help retard crack propagation (viz. a larger effective area along the $CaCO_3$-filled iPP interface to help absorb the impact energy) [16] which is in extremely good agreement with the result obtain in this study.

4.4.10 Morphology of Fractured Surface

Scanning electron microscopy (SEM) was used to observe the dispersion of $CaCO_3$ particles within the composites. In an attempt to do so, fractured surface of selected specimens after impact tests was investigated. Figure 4.17a to e shows SEM images of the fractured surface of selected impact test specimens for iPP composites filled with 30 wt.% of as-received, untreated,

admicellar-treated ([SDS]$_{equilibrium}$ = 200 μM), admicellar-treated ([SDS]$_{equilibrium}$ = 500 μM), and stearic acid-coated CaCO$_3$ particles, respectively. It is obvious that better dispersion with a low degree of agglomeration of the filler was observed with both stearic acid-coated and admicellar-treated CaCO$_3$-filled iPP composites.

The percentage of area of CaCO$_3$ particles on iPP matrix of the fractured surface of impact test specimens for the various types of CaCO$_3$-filled iPP composites are shown in Table 4.13.

When compared to the results obtained for iPP composites filled with untreated CaCO$_3$ particles, both stearic acid-coated and admicellar-treated (PP-coated) CaCO$_3$ resulted in the higher percentage area of CaCO$_3$ with the lower deviation (Figure 4.18). This result indicated that better dispersion was observed, as stated before.

In addition, the SEM images of the tensile test specimens sectioned along the direction of deformation for iPP filled with 30 wt.% of as-received, untreated, admicellar-treated ([SDS]$_{equilibrium}$ = 200 μM), admicellar-treated ([SDS]$_{equilibrium}$ = 500 μM), and stearic acid-coated CaCO$_3$ particles are shown in Figure 4.19a to e, respectively. It is also obvious from these micrographs that the adhesion between the treated CaCO$_3$ particles and the iPP matrix was not improved, suggesting that surface treatment of CaCO$_3$ particles by stearic acid-coated and admicellar-treated only helped the dispersion of the particles within the matrix.

4.5 Conclusions

In this study, admicellar polymerization of propylene can be conducted on CaCO$_3$ particles. The method was employed to form thin polypropylene films on the surface of CaCO$_3$. The CaCO$_3$ particle exhibited a PZC at 11.4 and anionic surfactant, SDS, was used with the solution pH adjusted to 8. The presence of a small amount of salt, sodium chloride, substantially improved the SDS adsorption on CaCO$_3$.

Evidence that a polypropylene coating had been formed on the CaCO$_3$ surface were (i) the propylene pressure drop that occurred during the adsolubilization

and admicellar polymerization processes, (ii) weight loss measurements, and (iii) FT-IR results.

Non-isothermal crystallization studied revealed that incorporation of $CaCO_3$ particles shifted the crystallization peak towards a higher temperature. Two types of crystallization exotherm were observed: the single-peak type and the double-peak type. The double-peak type was only found for iPP sample filled with 30 wt.% untreated $CaCO_3$ particles, which was postulated to be a result of self-nucleation effect of residue iPP crystallites entrapped along the rough surface of untreated $CaCO_3$ particles. Surface treatment of $CaCO_3$ particles with stearic acid-coated and admicellar-treated reduced the nucleating ability of the particles. WAXD results suggested that the incorporation of $CaCO_3$ affected the apparent degree of crystallinity. Moreover, surface-treated $CaCO_3$ resulted in the reduction of degree of crystallinity of iPP matrix.

The effects of $CaCO_3$ with various types of surface treatment (untreated, stearic acid-coated, and admicellar-treated) on mechanical properties (tensile, flexural, and impact properties) of $CaCO_3$-filled iPP composites were investigated. Both stearic acid-coated and admicellar-treated $CaCO_3$ resulted in the reduction of both the tensile strength at yield, strain at yield, and the Young's modulus of the $CaCO_3$-filled iPP composites when compared with untreated $CaCO_3$. Similar results were shown for flexural strength. On the other hand, the impact strength of composites filled with stearic acid-coated and admicellar-treated $CaCO_3$ was higher than untreated $CaCO_3$. SEM studies indicated better dispersion and decreased agglomeration of the filler upon surface treatment of $CaCO_3$. These results clearly demonstrated that surface treatment of $CaCO_3$ particles with stearic acid-coated and admicellar-treated mainly helped the dispersion of the particles within the iPP matrix.

4.6 Acknowledgements

4.7 References

[1]   Osman, M.A., and Suter, U.W. (2002) Surface treatment of calcite with fatty acids: structure and properties of the organic monolayer. Chemical Mater, 14, 4408-4415.

[2]   Chan, C.M., Wu, J., Li, J.X., and Cheung, Y.K. (2002) Polypropylene/calcium carbonate nanocomposites. Polymer, 43, 2981-2992.

[3]   Thio, Y.S., Argon, A.S., Cohen, R.E., and Weinberg, M. (2002) Toughening of isotactic polypropylene with CaCO$_3$ particles. Polymer, 43, 3661-3674.

[4]   Sitthitham, B., Yanumet, N., Ellis, J.W., Grady, B.P., and O'Rear, E.A. (2001) Coating of Glass Fiber to Improve Adhesion in Glass Fiber Reinforced Polyethylene. M.S. Thesis in Polymer Science, The Petroleum and Petrochemical College, Chulalongkorn University.

[5]   Martínez-Luévanos, A., Uribe-Salas, A., López-Valdivieso, A. (1999) Mechanism of adsorption of sodium dodecylsulfonate on celestite and calcite. Minerals Engineering, 12, 919-936.

[6]   Pongprayoon, T., Yanumet, N., and O'Rear, E.A. (2002) Admicellar polymerization of styrene on cotton. Journal of Colloid and Interface Science, 249, 227-234.

[7]   Pukánszky, B. and Fekete, E. (1998) Aggregation tendency of particulate fillers: determination and consequences. Polymers & Polymer Composites, 6, 313-322.

[8]   Supaphol, P. and Harnsiri, W. (2003) Effects of calcium carbonate and its purity on crystallization and melting behavior, mechanical properties, and processability of syndiotactic poly(propylene). Journal of Applied Polymer Science, submitted.

[9] Cho, K., Saheb, D.N., Choi, J., and Yang, H. (2002) Real time in situ X-ray diffraction studies on the melting memory effect in the crystallization of β-isotactic polypropylene. Polymer, 43, 1407-1416.

[10] Zhang, Q.X., Yu, Z.Z., Xie X.L., and Mai, Y.W. (2004) Crystallization and impact energy of polypropylene/CaCO$_3$ nanocomposites with nonionic modifier. Polymer, 45, 5985-5994.

[11] Tuner-Jones, A., Aixlewood, J.M., and Beckett, D.R. (1964) Makromolecular Chemistry, 75, 134.

[12] Rybnikar, F. (1991) Interaction in the system isotactic polypropylene-calcite. Journal of Applied Polymer Science, 42, 2727-2737.

[13] González, J., Albano, C., Ichazo, M., and Díaz, B. (2002) Effects of coupling agents on mechanical and morphological behavior of the PP/HDPE blend with two different CaCO$_3$. European Polymer Journal, 38, 2465-5475.

[14] Maiti, S.N., and Mahapatro, P.K. (1991) Mechanical properties of iPP/CaCO$_3$ composites. Journal of Applied Polymer Science, 42, 3101-3110.

[15] Silva, A.L.N., Rocha, M.C.G., Moraes, M.A.R., Valente, C.A.R., and Coutinho, F.M.B. (2002) Mechanical and rheological properties of composites based on polyolefin and mineral additives. Polymer Testing, 21, 57-60.

[16] Riley, A.M., Paynter, C.D., McGenity, P.M., and Adams, J.M. (1990) Plastic and Rubber Processing and Applications, 14, 85.
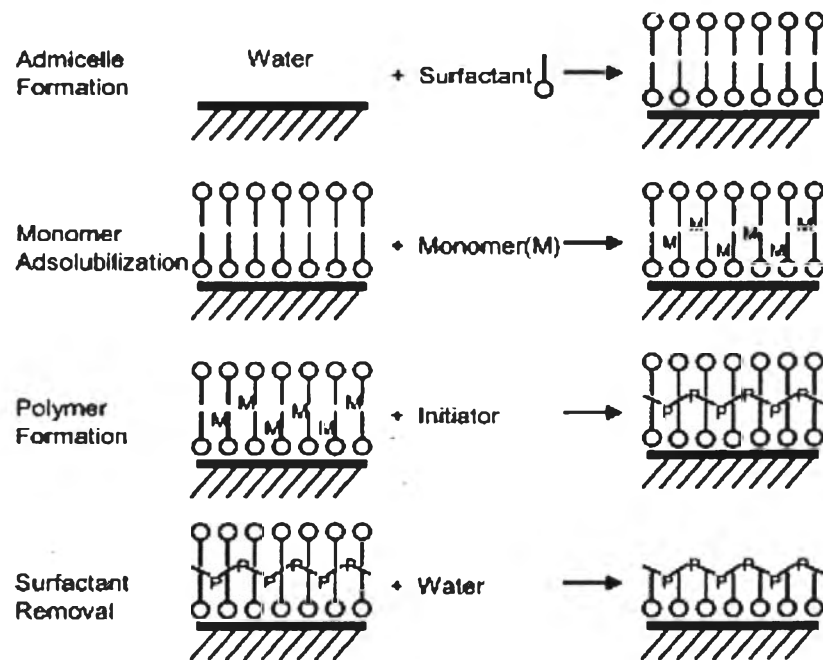
Figure 4.1 Schematic of four steps admicellar polymerization process.
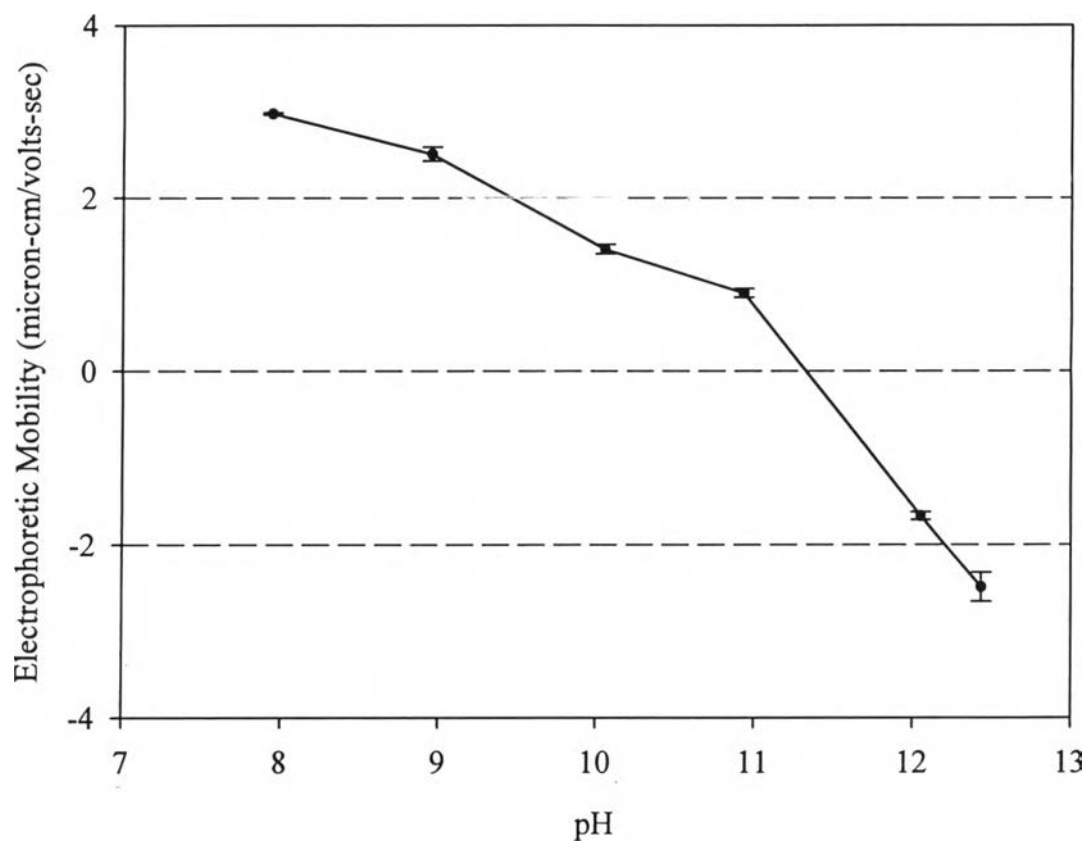
Figure 4.2 The electrophoretic mobility of CaCO₃ particles in aqueous solution at various pH.
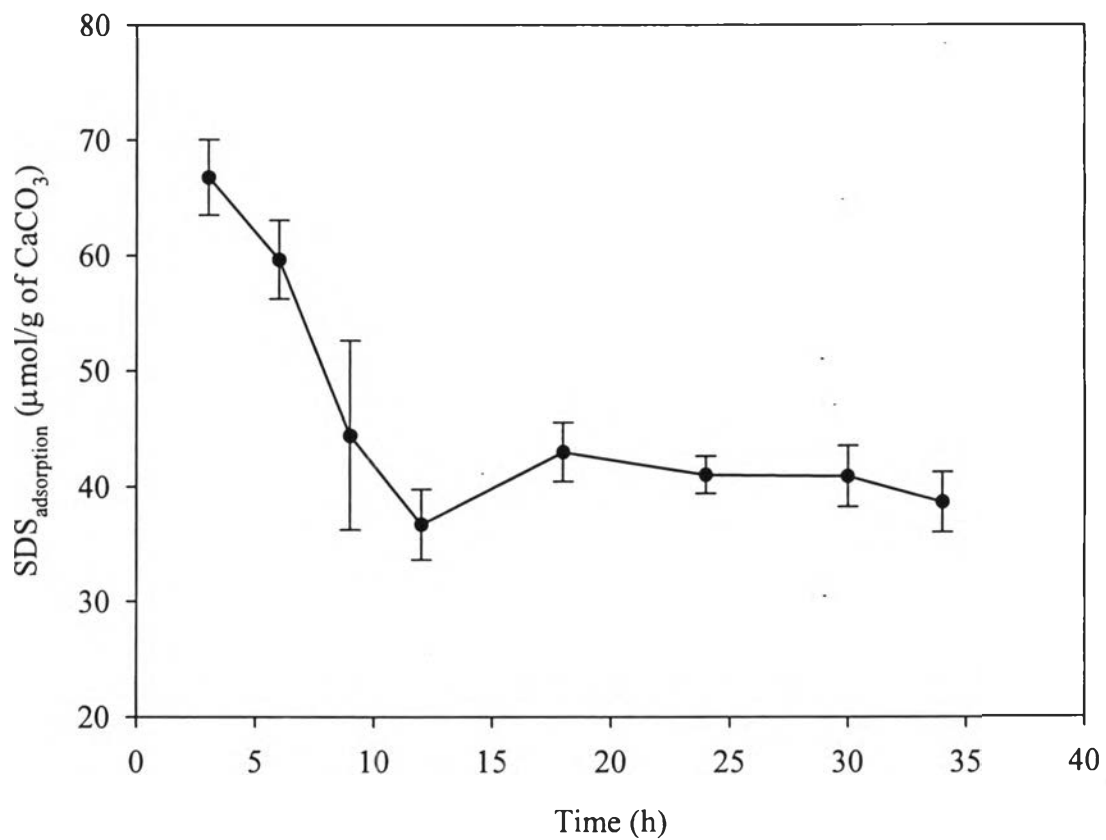
Figure 4.3 The equilibrium time for SDS adsorption on $CaCO_3$.
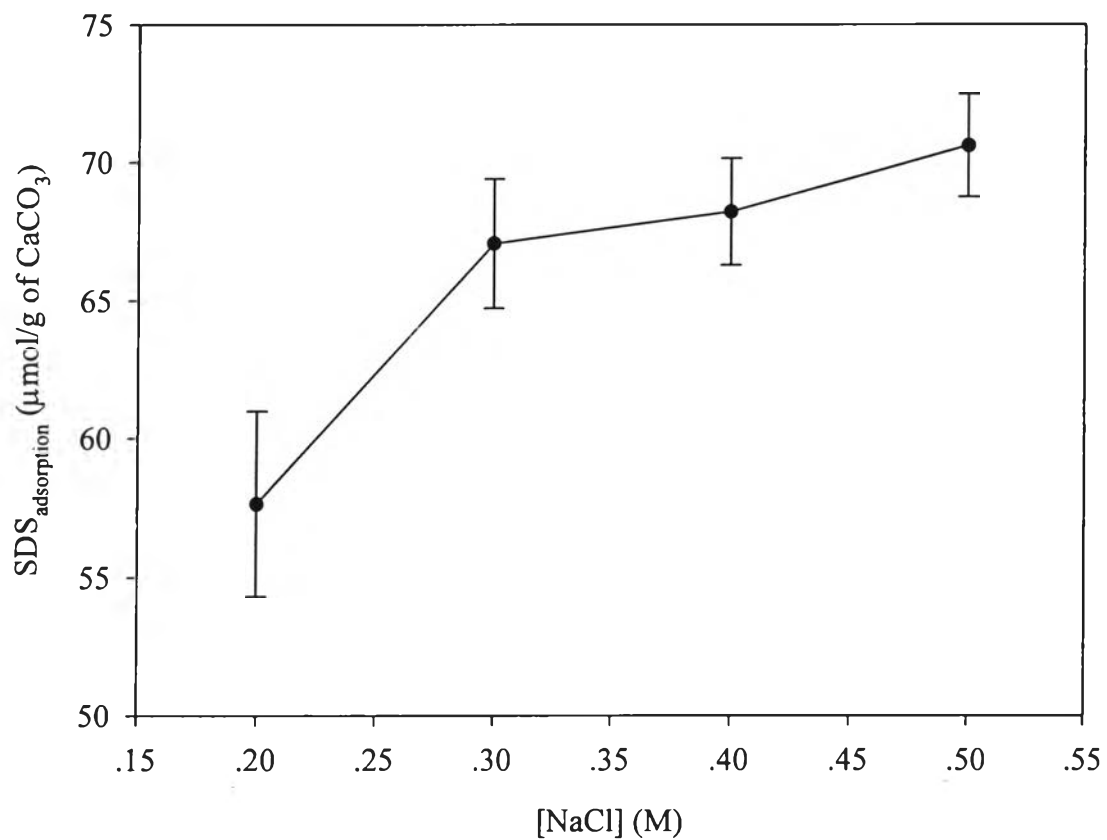
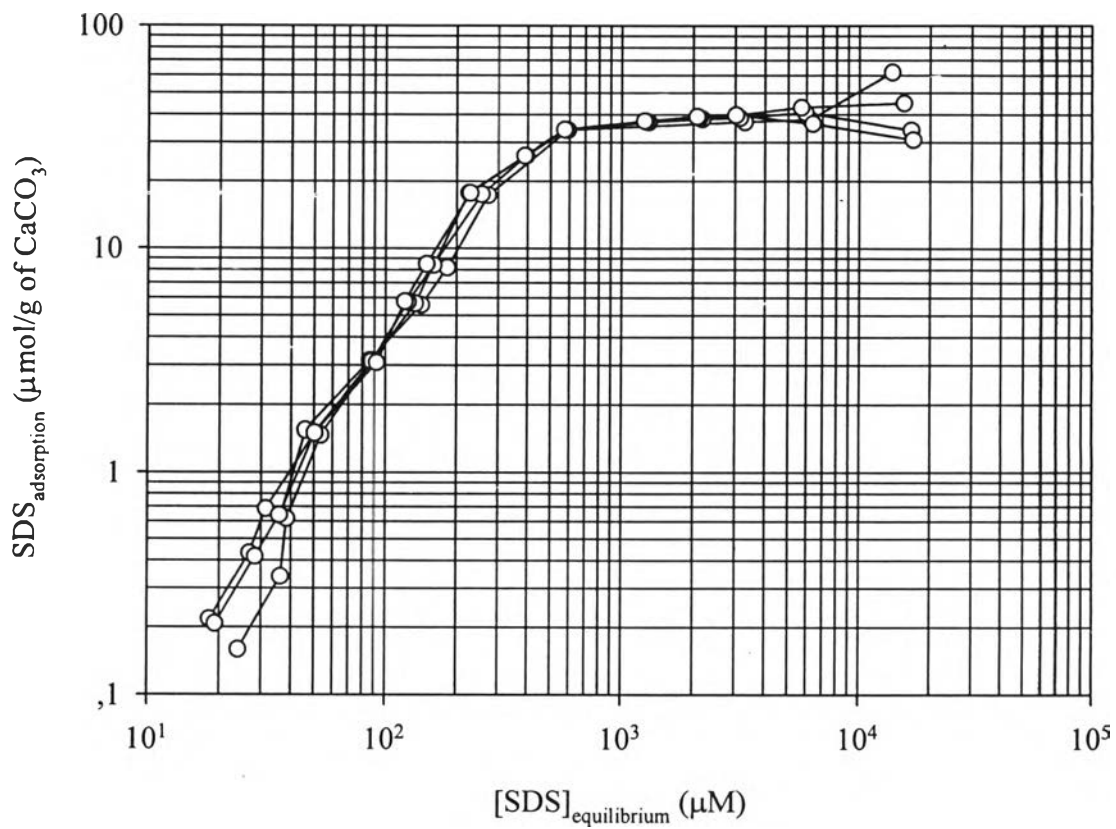**Figure 4.4** The effect of electrolyte on the amount of SDS adsorption on $CaCO_3$.

Figure 4.5 The adsorption isotherm of SDS on $CaCO_3$ pH 8 and a salt concentration of 0.3 M.

Table 4.1 Summary of propylene pressure drop values for the blank system and the admicellar polymerization system

Admicellar polymerization condition	Propylene pressure drop ($MPa \times 10^3$)		
	Blank	System	$\triangle P$
$[SDS]_{equilibrium} = 200\ \mu M$, $SDS_{adsorption} = 15\ \mu mol/g$ of $CaCO_3$	6.89	39.6432	75
$[SDS]_{equilibrium} = 500\ \mu M$, $SDS_{adsorption} = 30\ \mu mol/g$ of $CaCO_3$	6.89	48.2641	31
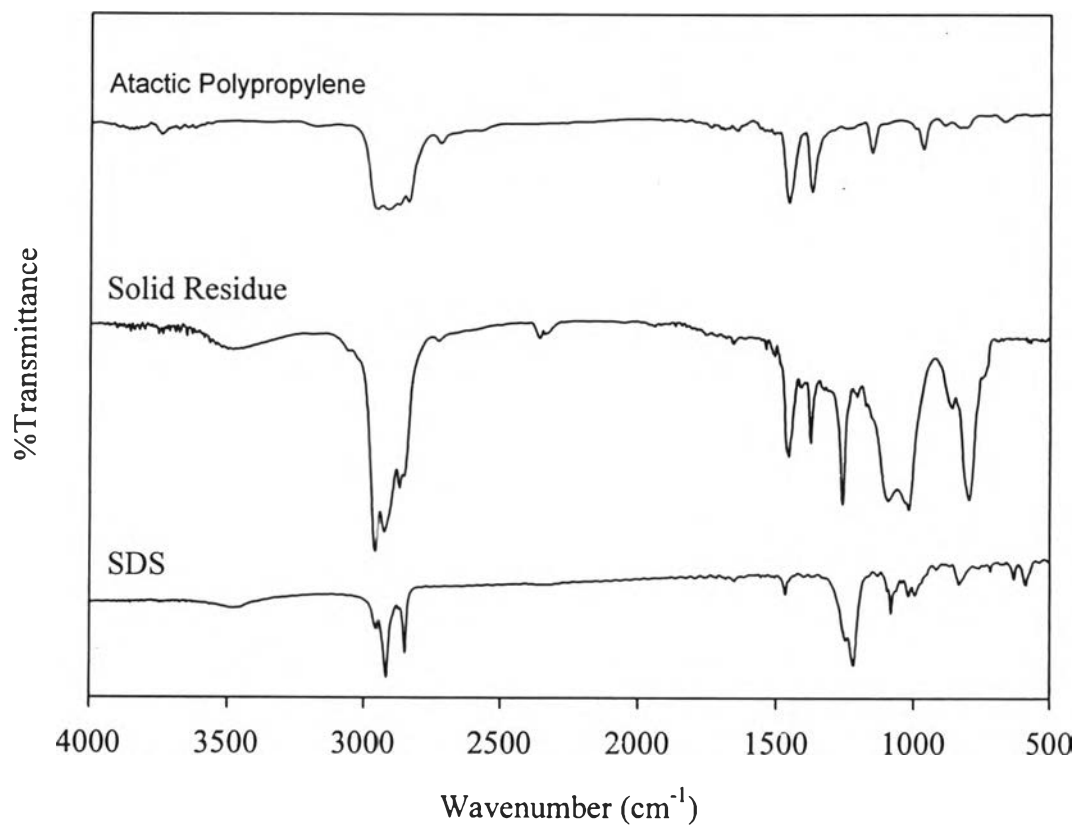
Figure 4.6a The FT-IR spectra of atactic polypropylene, solid residue, and SDS.
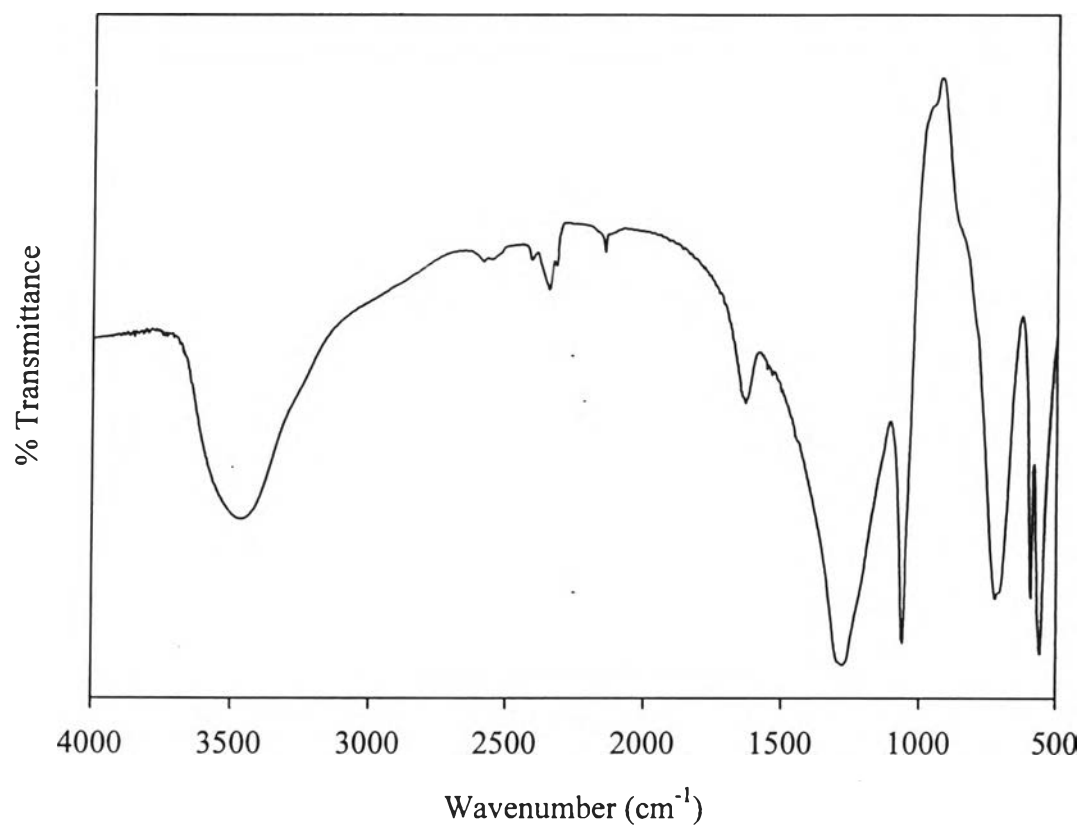
Figure 4.6b The FT-IR spectrum of initiator ($Na_2S_2O_8$).

Table 4.2 Assignment of characteristic peaks from FT-IR spectrum of solid residue

Wavenumber (cm^{-1})	Assignment
2960	symmetrical C–H stretching vibration of –CH_3 group
2930	asymmetrical C–H stretching vibration of –CH_2– group
2870	asymmetrical C–H stretching vibration of –CH_3 group
2850	symmetrical C–H stretching vibration of –CH_2– group
1470	symmetrical C–H scissoring vibration of –CH_2– group
	asymmetrical C–H bending vibration of –CH_3 group
1380	symmetrical C–H bending vibration of –CH_3 group
1220-1300	asymmetrical stretching vibrational band of RO–$SO_3^-M^+$
1050-1120	symmetrical stretching vibrational band of RO–$SO_3^-M^+$
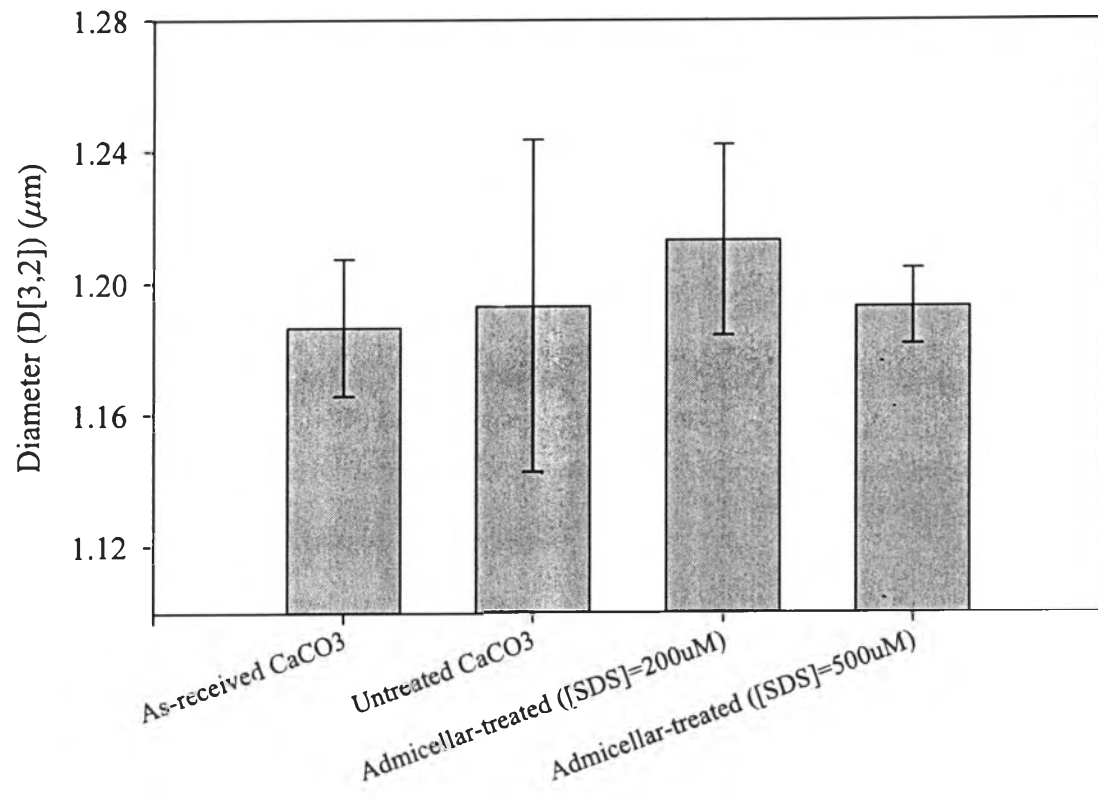
Figure 4.7 The particle size results of the various types of surface-treated CaCO₃.

Table 4.3 Summary of percentage of weight loss values for the various types of surface-treated $CaCO_3$

Type of surface-treated $CaCO_3$	Weight loss (%)
As-received $CaCO_3$	0.8568 ± 0.1092
Stearic acid-coated $CaCO_3$	5.6991 ± 0.3737
Untreated $CaCO_3$	0.5882 ± 0.1652
Admicellar-treated $CaCO_3$ ($[SDS]_{equilibrium} = 200 \ \mu M$)	0.6609 ± 0.0916
Admicellar-treated $CaCO_3$ ($[SDS]_{equilibrium} = 500 \ \mu M$)	0.7584 ± 0.0645
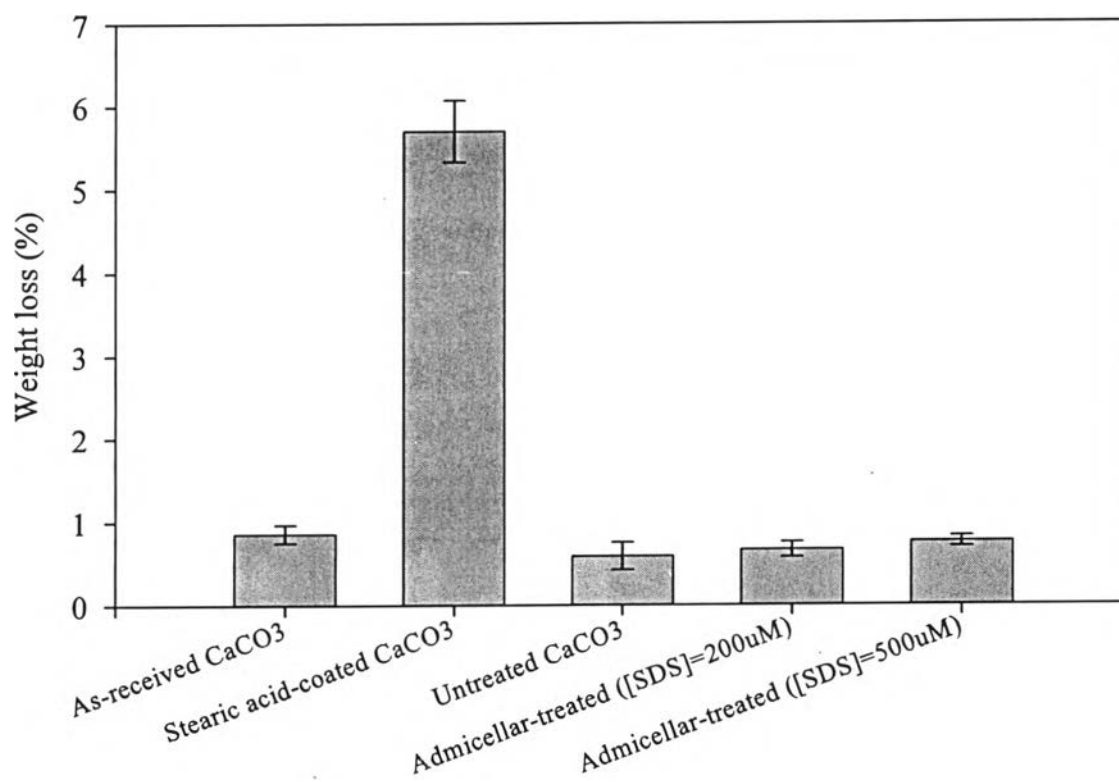
Figure 4.8 The percentage of weight loss of the various types of surface-treated CaCO₃.
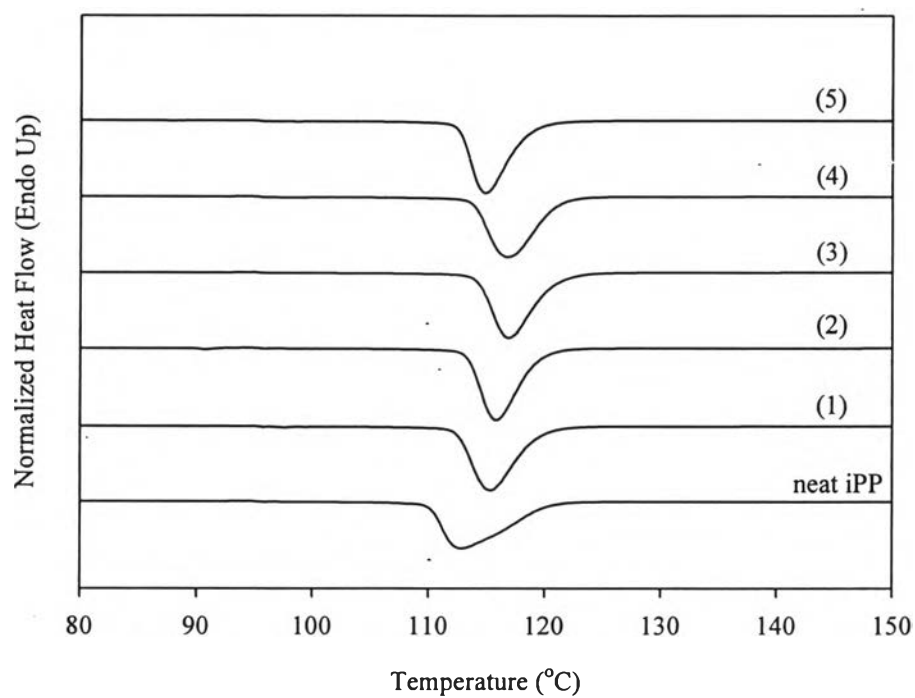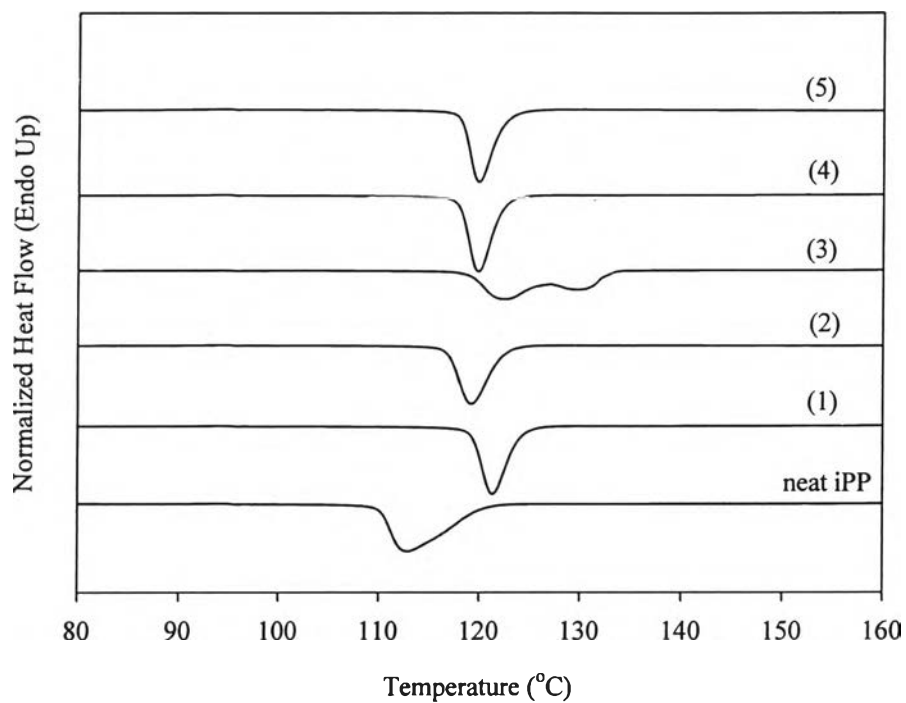
Figure 4.9a The non-isothermal crystallization exotherms for neat iPP and 2 wt.% $CaCO_3$ filled iPP samples with various types of surface treatment of $CaCO_3$: (1) as-received, (2) stearic acid-coated, (3) untreated, (4) admicellar-treated ([SDS]$_{equilibrium}$ = 200 μM), and (5) admicellar-treated ([SDS]$_{equilibrium}$ = 500 μM).

Figure 4.9b The non-isothermal crystallization exotherms for neat iPP and 30 wt.% $CaCO_3$ filled iPP samples with various types of surface treatment of $CaCO_3$: (1) as-received, (2) stearic acid-coated, (3) untreated, (4) admicellar-treated ($[SDS]_{equilibrium}$ = 200 μM), and (5) admicellar-treated ($[SDS]_{equilibrium}$ = 500 μM).

Table 4.4 Summary of non-isothermal crystallization characteristics observed for all of the samples studied

| Sample	CaCO$_3$ Content (wt.%)	Crystallization Characteristic			
		$T_{c,onset}$ (°C)	T_{cl} (°C)	T_{ch} (°C)	ΔH_f^o (J/g)
Neat iPP	0	120.4	112.8	-	97.1
As-received CaCO$_3$-filled iPP	2	119.4	115.3	-	96.7
	30	124.0	121.3	-	71.8
Stearic acid-coated CaCO$_3$-filled iPP	2	119.4	115.8	-	95.6
	30	122.3	119.2	-	65.4
Untreated CaCO$_3$-filled iPP	2	120.9	116.8	-	95.9
	30	127.9	122.5	129.8	72.6
Admicellar-treated CaCO$_3$-filled iPP ([SDS]$_{equilibrium}$ = 200 μM)	2	120.1	116.8	-	96.1
	30	122.4	119.8	-	74.0
Admicellar-treated CaCO$_3$-filled iPP ([SDS]$_{equilibrium}$ = 500 μM)	2	118.6	114.8	-	95.7
	30	122.4	119.8	-	63.7
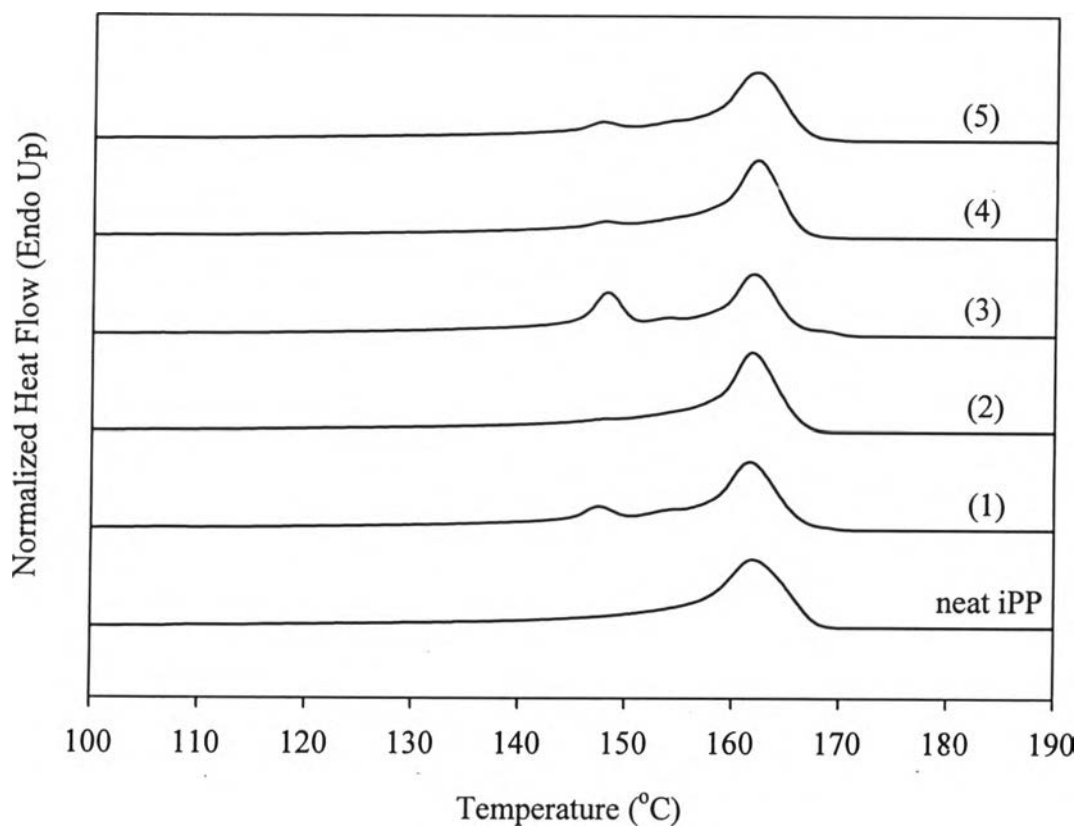
Figure 4.10a The subsequent melting endotherms for neat iPP and 2 wt.% CaCO$_3$ filled iPP samples with various types of surface treatment of CaCO$_3$: (1) as-received, (2) stearic acid-coated, (3) untreated, (4) admicellar-treated ([SDS]$_{equilibrium}$ = 200 µM), and (5) admicellar-treated ([SDS]$_{equilibrium}$ = 500 µM).
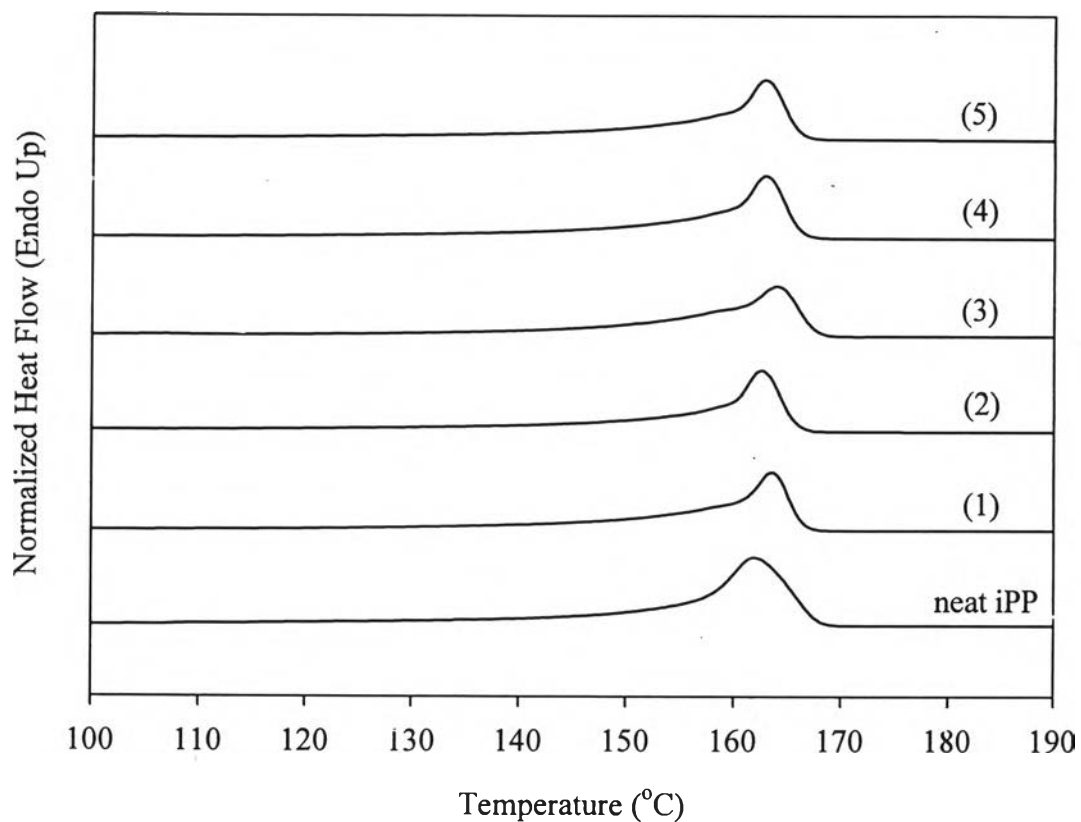
Figure 4.10b The subsequent melting endotherms for neat iPP and 30 wt.% CaCO$_3$ filled iPP samples with various types of surface treatment of CaCO$_3$: (1) as-received, (2) stearic acid-coated, (3) untreated, (4) admicellar-treated ([SDS]$_{equilibrium}$ = 200 μM), and (5) admicellar-treated ([SDS]$_{equilibrium}$ = 500 μM).

Tabie 4.5 Summary of subsequent melting characteristics observed for all of the samples studied

| Sample	$CaCO_3$ Content (wt.%)	Melting Characteristic			
		$T_{m,onset}$ (°C)	T_{ml} (°C)	T_{mh} (°C)	ΔH_f^o (J/g)
Neat iPP	0	156.0	-	162.0	98.6
As-received $CaCO_3$-filled iPP	2	156.8	147.4	161.7	96.6
	30	159.1	-	163.4	72.9
Stearic acid-coated $CaCO_3$-filled iPP	2	157.5	-	161.7	96.0
	30	158.6	-	162.4	72.3
Untreated $CaCO_3$-filled iPP	2	157.7	148.0	161.7	97.9
	30	158.0	-	164.0	72.7
Admicellar-treated $CaCO_3$-filled iPP ([SDS]$_{equilibrium}$ = 200 μM)	2	157.5	147.7	162.0	96.4
	30	158.8	-	162.7	75.0
Admicellar-treated $CaCO_3$-filled iPP ([SDS]$_{equilibrium}$ = 500μM)	2	156.7	147.4	162.0	95.7
	30	158.8	-	162.7	73.6
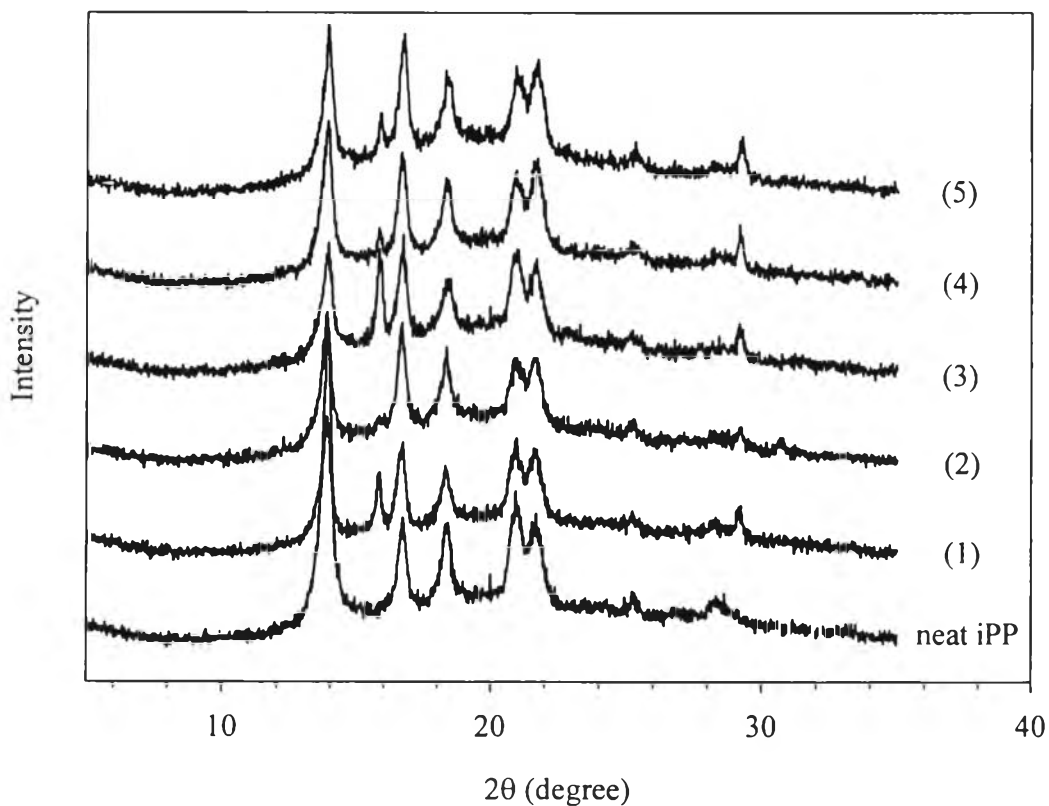
Figure 4.11a The WAXD patterns for neat iPP and 2 wt.% $CaCO_3$ filled iPP samples with various types of surface treatment of $CaCO_3$: (1) as-received, (2) stearic acid-coated, (3) untreated, (4) admicellar-treated ($[SDS]_{equilibrium}$ = 200 μM), and (5) admicellar-treated ($[SDS]_{equilibrium}$ = 500 μM).
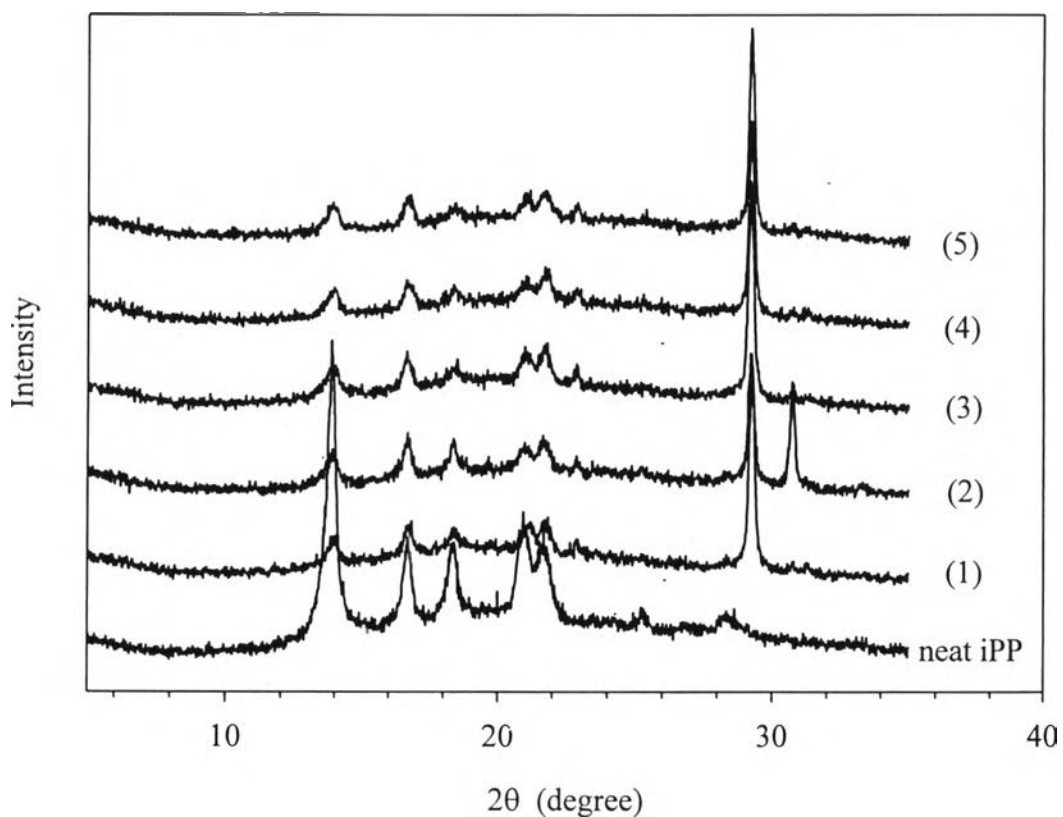
Figure 4.11b The WAXD patterns for neat iPP and 30 wt.% $CaCO_3$ filled iPP samples with various types of surface treatment of $CaCO_3$: (1) as-received, (2) stearic acid-coated, (3) untreated, (4) admicellar-treated ($[SDS]_{equilibrium}$ = 200 μM), and (5) admicellar-treated ($[SDS]_{equilibrium}$ = 500 μM).

Table 4.6 The K_β values of 2 wt.% as-received, untreated, and admicellar-treated $CaCO_3$-filled iPP composites

Sample	K_β
2 wt.% as-received $CaCO_3$-filled iPP composite	0.21
2 wt.% untreated $CaCO_3$-filled iPP composite	0.27
2 wt.% admicellar-treated $CaCO_3$-filled iPP composite ($[SDS]_{equilibrium}$ = 200 µM)	0.16
2 wt.% admicellar-treated $CaCO_3$-filled iPP composite ($[SDS]_{equilibrium}$ = 500 µM)	0.18

Table 4.7 Summary of WAXD degree of crystallinity for all of the samples studied

Sample	$CaCO_3$ Content (wt.%)	χ^{WAXD} (%)
Neat iPP	0	36.8
As-received $CaCO_3$-filled iPP	2	29.2
	30	20.9
Stearic acid-coated $CaCO_3$-filled iPP	2	30.4
	30	25.0
Untreated $CaCO_3$-filled iPP	2	30.4
	30	25.3
Admicellar-treated $CaCO_3$-filled iPP ($[SDS]_{equilibrium} = 200\ \mu M$)	2	30.2
	30	18.9
Admicellar-treated $CaCO_3$-filled iPP ($[SDS]_{equilibrium} = 500\ \mu M$)	2	29.2
	30	18.8

Table 4.8 Summary of tensile strength at yield values of the various types of surface-treated $CaCO_3$-filled iPP composites

Type of surface-treated $CaCO_3$ used in composites	Tensile strength at yield (MPa)
As-received $CaCO_3$	26.20 ± 0.62
Stearic acid-coated $CaCO_3$	26.71 ± 0.54
Untreated $CaCO_3$	26.77 ± 0.18
Admicellar-treated $CaCO_3$ ($[SDS]_{equilibrium} = 200$ μM)	26.17 ± 0.18
Admicellar-treated $CaCO_3$ ($[SDS]_{equilibrium} = 500$ μM)	25.60 ± 0.21

Table 4.9 Summary of strain at yield values of the various types of surface-treated $CaCO_3$-filled iPP composites

Type of surface-treated $CaCO_3$ used in composites	Strain at yield (%)
As-received $CaCO_3$	4.56 ± 0.28
Stearic acid-coated $CaCO_3$	4.89 ± 0.36
Untreated $CaCO_3$	3.83 ± 0.11
Admicellar-treated $CaCO_3$ ($[SDS]_{equilibrium} = 200$ μM)	4.76 ± 0.23
Admicellar-treated $CaCO_3$ ($[SDS]_{equilibrium} = 500$ μM)	4.64 ± 0.24

Table 4.10 Summary of Young's modulus values of the various types of surface-treated $CaCO_3$-filled iPP composites

Type of surface-treated $CaCO_3$ used in composites	Young's modulus (MPa)
As-received $CaCO_3$	2484.97 ± 180.64
Stearic acid-coated $CaCO_3$	2648.29 ± 307.70
Untreated $CaCO_3$	2808.12 ± 359.79
Admicellar-treated $CaCO_3$ ($[SDS]_{equilibrium} = 200 \ \mu M$)	2569.71 ± 291.19
Admicellar-treated $CaCO_3$ ($[SDS]_{equilibrium} = 500 \ \mu M$)	2414.22 ± 247.88
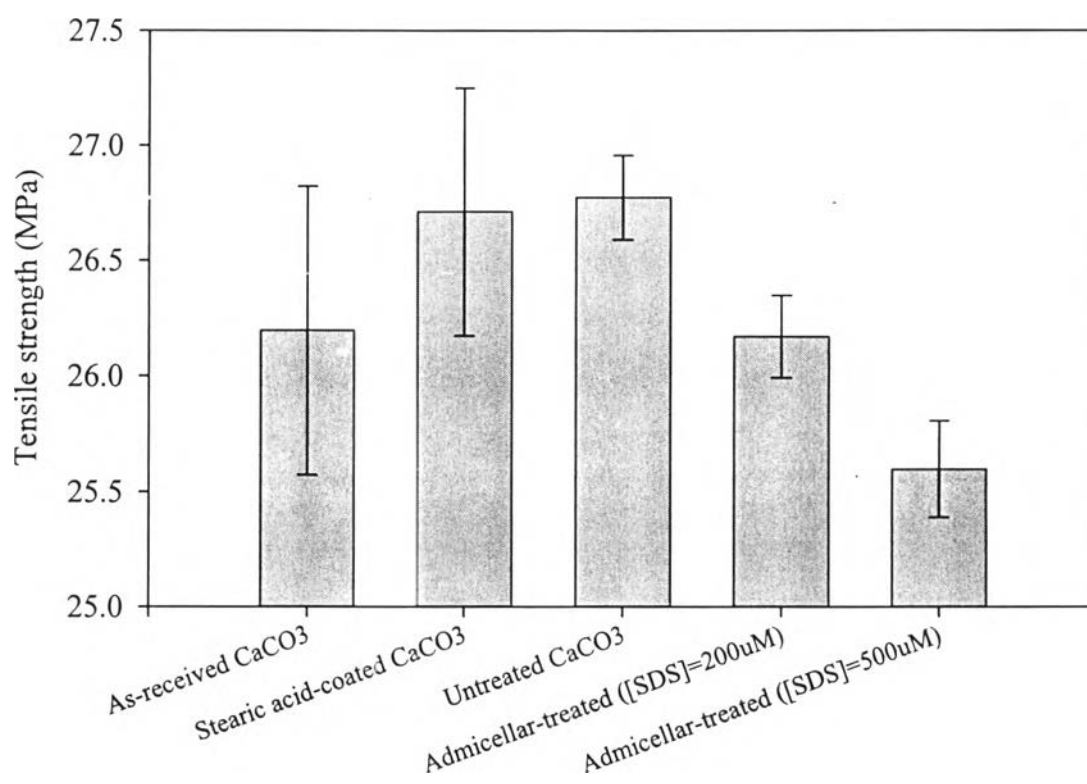
Figure 4.12 The tensile strength at yield of the various types of surface-treated CaCO$_3$-filled iPP composites.
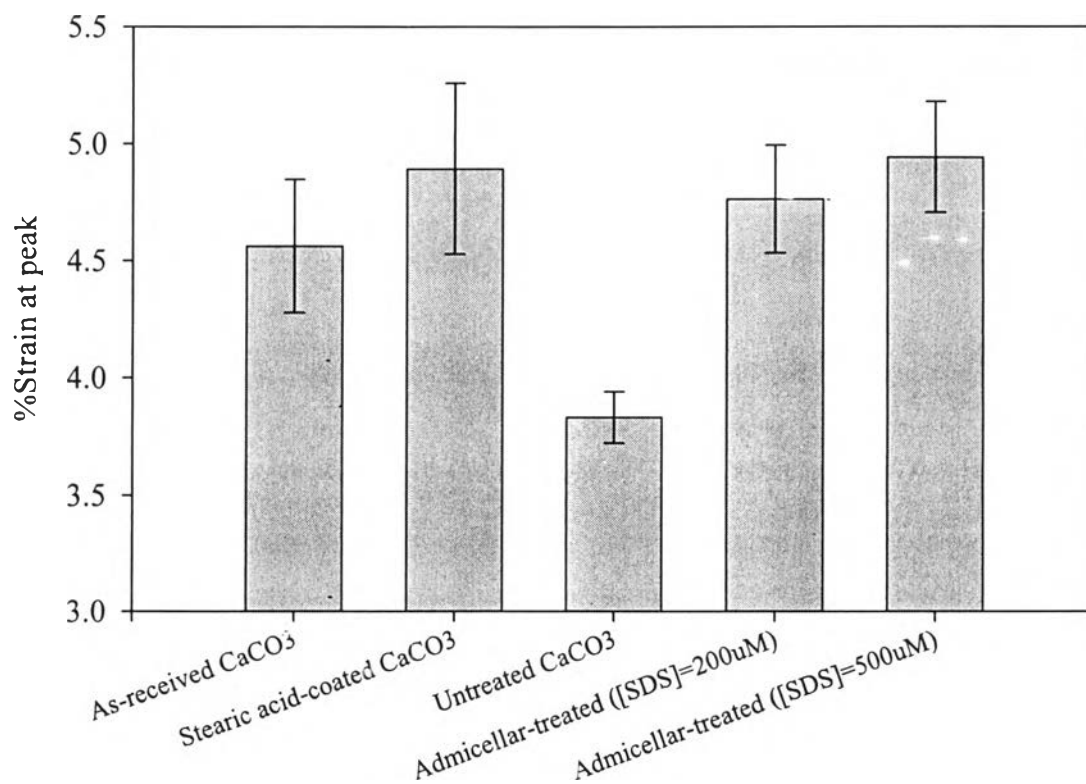
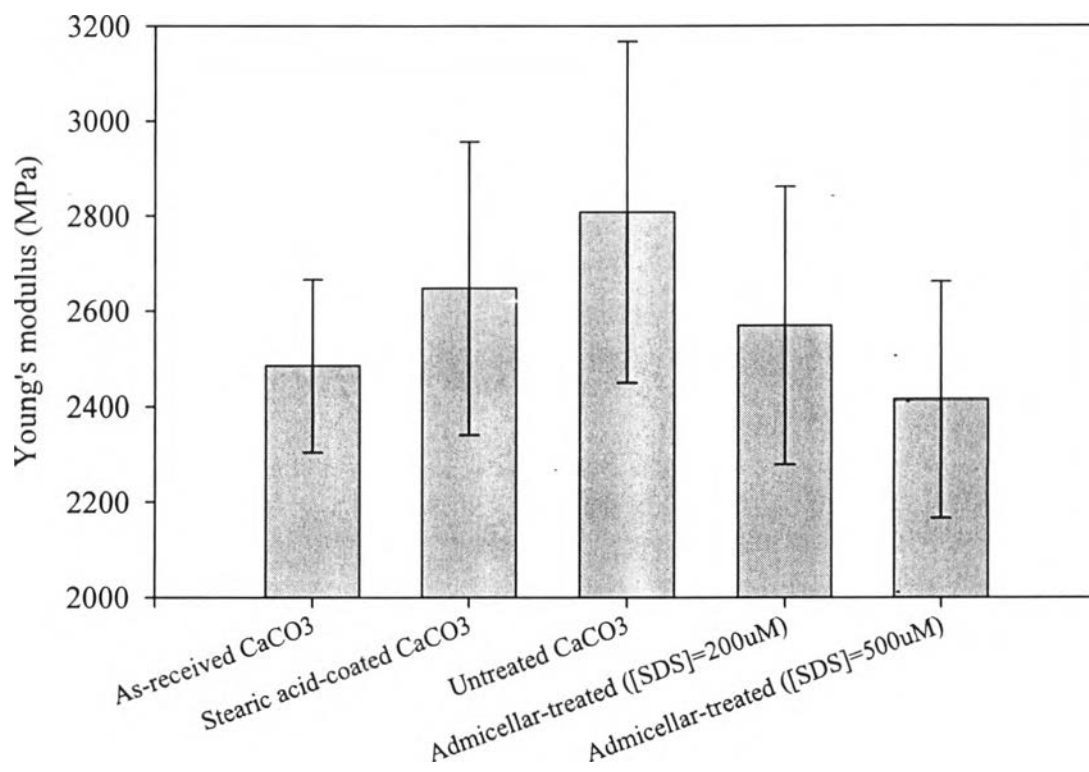**Figure 4.13** The strain at yield of the various types of surface-treated CaCO₃-filled iPP composites.

Figure 4.14 The Young's modulus of the various types of surface-treated $CaCO_3$-filled iPP composites.

Table 4.11 Summary of flexural strength values of the various types of surface-treated $CaCO_3$-filled iPP composites

Type of surface-treated $CaCO_3$ used in composites	Flexural strength (MPa)
As-received $CaCO_3$	35.53 ± 0.75
Stearic acid-coated $CaCO_3$	36.26 ± 0.85
Untreated $CaCO_3$	40.49 ± 0.92
Admicellar-treated $CaCO_3$ ($[SDS]_{equilibrium} = 200$ μM)	36.43 ± 1.27
Admicellar-treated $CaCO_3$ ($[SDS]_{equilibrium} = 500$ μM)	36.59 ± 0.48
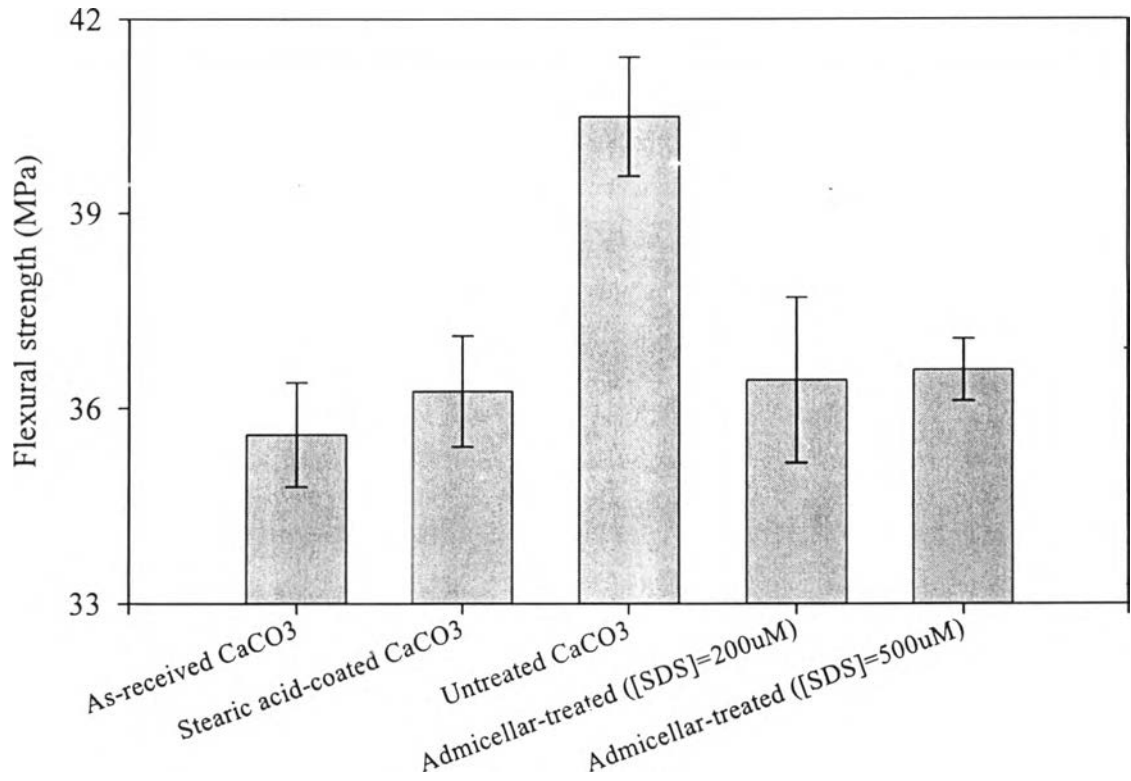
Figure 4.15 The flexural strength of the various types of surface-treated $CaCO_3$-filled iPP composites.

Table 4.12 Summary of impact strength values of the various types of surface-treated $CaCO_3$-filled iPP composites

Type of surface-treated $CaCO_3$ used in composites	Impact strength (J/m)
As-received $CaCO_3$	33.73 ± 3.04
Stearic acid-coated $CaCO_3$	40.10 ± 2.62
Untreated $CaCO_3$	29.81 ± 3.44
Admicellar-treated $CaCO_3$ ([SDS]$_{equilibrium}$ = 200 μM)	32.21 ± 3.99
Admicellar-treated $CaCO_3$ ([SDS]$_{equilibrium}$ = 500 μM)	32.97 ± 4.01
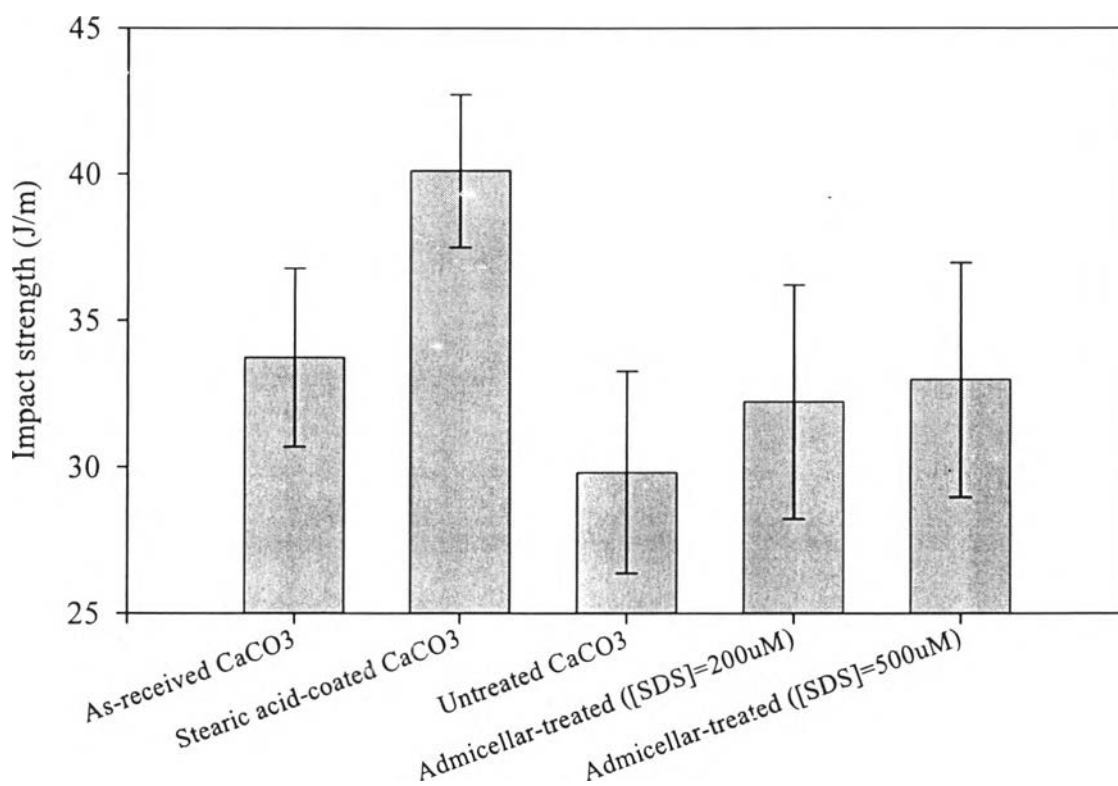
Figure 4.16 The impact strength of the various types of surface-treated $CaCO_3$-filled iPP composites.
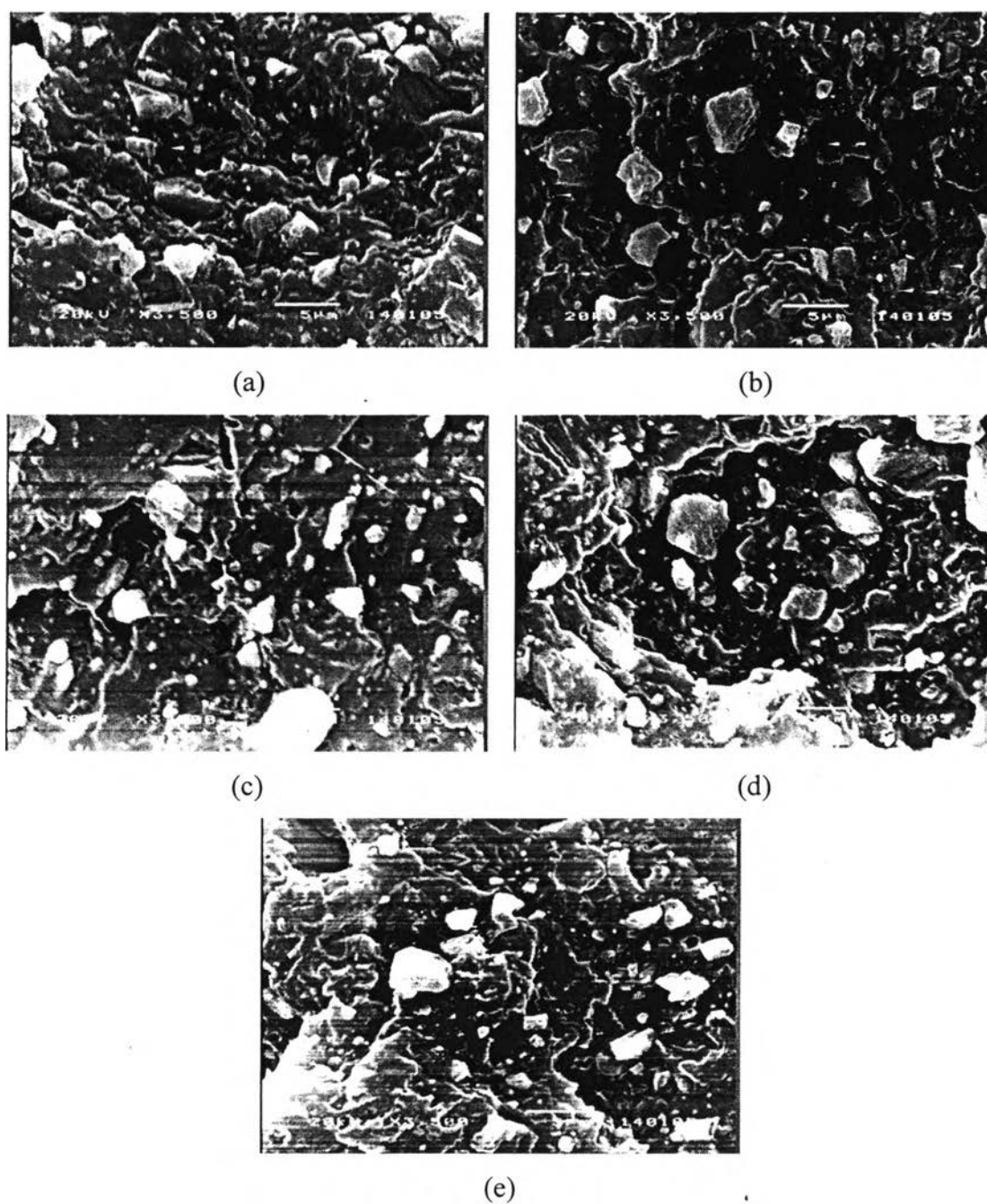
Figure 4.17 The SEM micrographs of the fractured surface of selected impact test specimens for iPP filled with 30 wt.%: (a) as-received, (b) untreated, (c) admicellar-treated ([SDS]$_{equilibrium}$ = 200 μM), (d) admicellar-treated ([SDS]$_{equilibrium}$ = 500 μM), and (e) stearic acid-coated $CaCO_3$ particles.

Table 4.13 Summary of percentage of area values of the various types of surface-treated $CaCO_3$ on iPP matrix of the fractured surface of impact test specimens for 30 wt.% $CaCO_3$-filled iPP composites

Type of surface-treated $CaCO_3$	Area of $CaCO_3$ on iPP matrix (%)
As-received $CaCO_3$	8.28 ± 0.53
Stearic acid-coated $CaCO_3$	9.56 ± 0.39
Untreated $CaCO_3$	7.78 ± 0.57
Admicellar-treated $CaCO_3$ ([SDS]$_{equilibrium}$ = 200 µM)	8.49 ± 0.52
Admicellar-treated $CaCO_3$ ([SDS]$_{equilibrium}$ = 500 µM)	8.96 ± 0.44

Remark: average percentage of area values were calculated from 8 SEM images (x3,500)
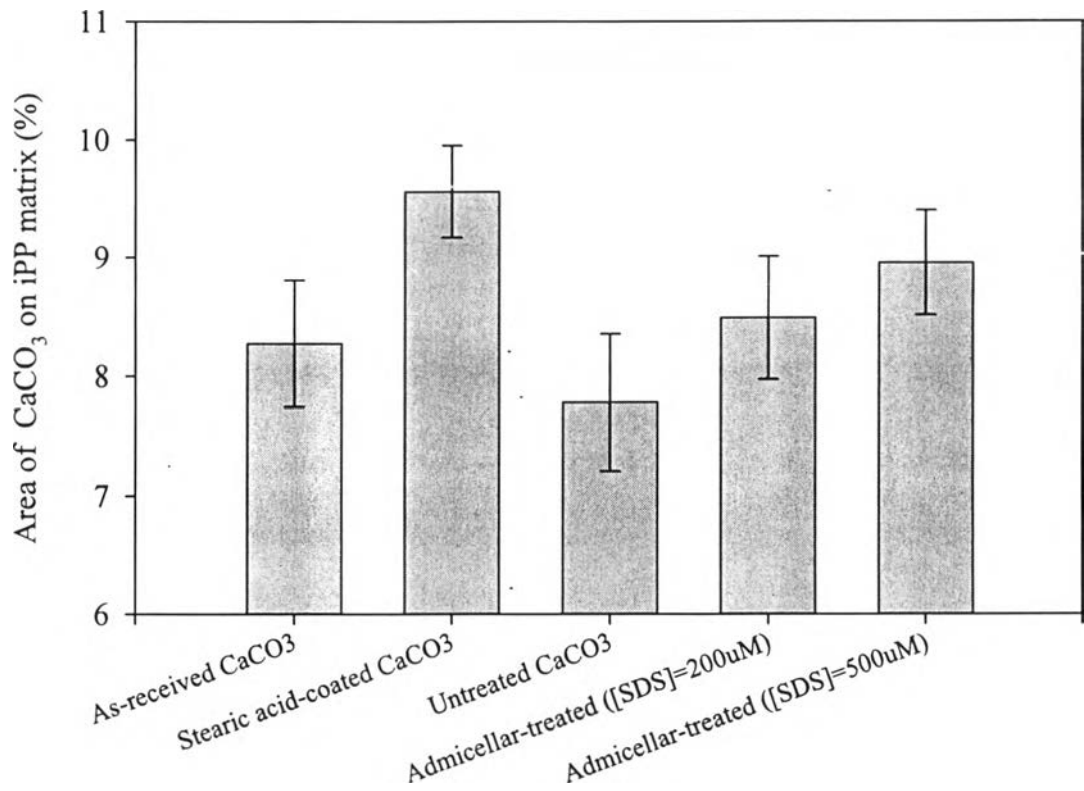
Figure 4.18 The percentage of area of $CaCO_3$ on iPP matrix of the fractured surface of impact test specimens for the various types of surface-treated $CaCO_3$-filled iPP composites.
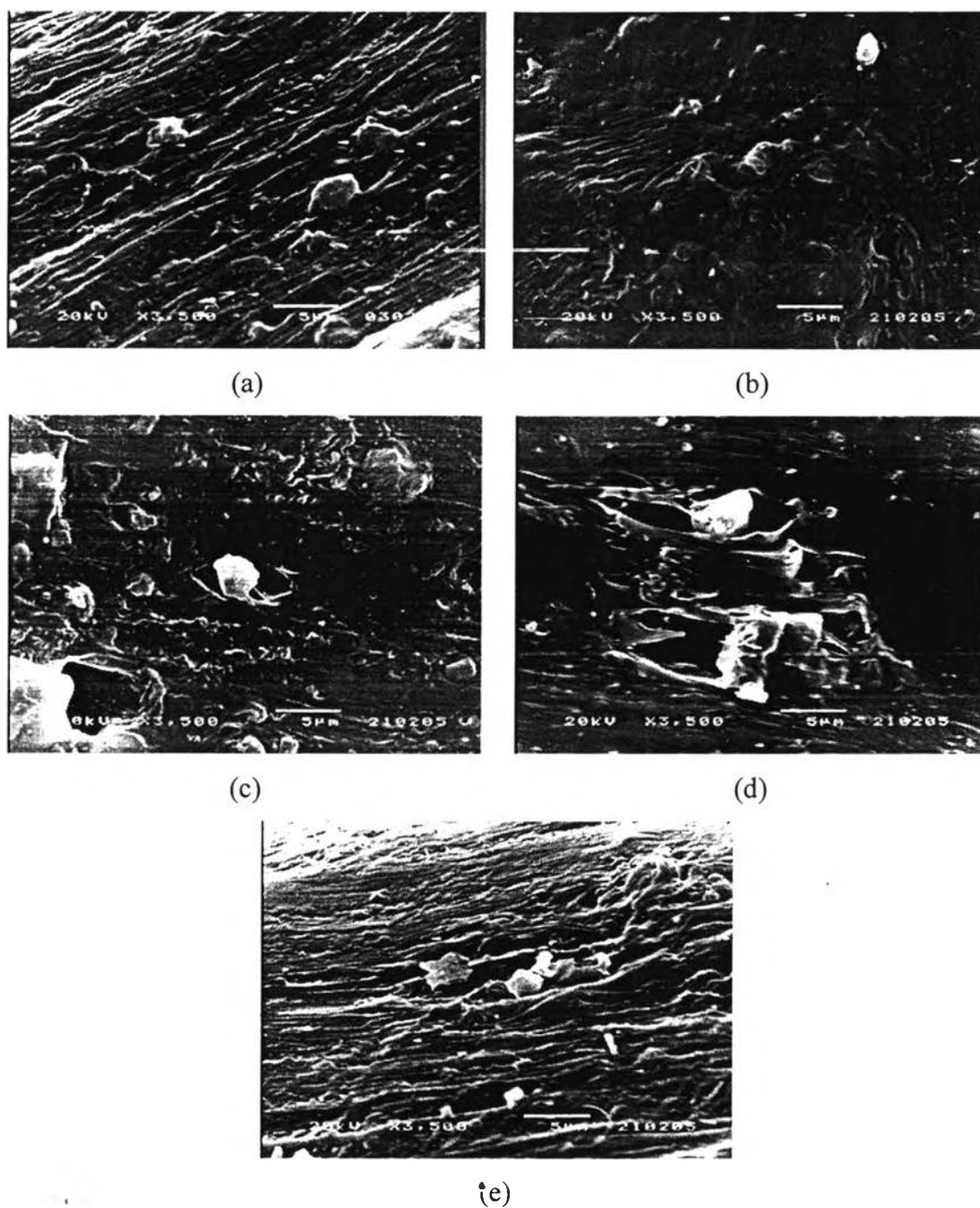
(a)

(b)

(c)

(d)

(e)

Figure 4.19 The SEM micrographs of the tensile test specimens sectioned along the direction of deformation for iPP filled with 30 wt.%: (a) as-received, (b) untreated, (c) admicellar-treated ($[SDS]_{equilibrium}$ = 200 μM), (d) admicellar-treated ($[SDS]_{equilibrium}$ = 500 μM), and (e) stearic acid-coated $CaCO_3$ particles.